Estimating the R-Star in the US: A Score-Driven State-Space Model with Time-Varying Volatility Persistence

Pál, Tibor and Storti, Giuseppe

University of Salerno, DISES

14 July 2025

Estimating the R-Star in the US: A Score-Driven State-Space Model with Time-Varying Volatility Persistence

Tibor Pál Giuseppe Storti*

Università degli Studi di Salerno, DISES

Abstract

This paper analyses the dynamics of the natural rate of interest (r-star) in the US using a score-driven state-space model within the Laubach–Williams structural framework. Compared to standard score-driven specifications, the proposed model enhances flexibility in variance adjustment by assigning time-varying weights to both the conditional likelihood score and the inertia coefficient in the volatility updating equations. The improved state dependence of volatility dynamics effectively accounts for sudden shifts in volatility persistence induced by highly volatile unexpected events. In addition, allowing time variation in the IS and Phillips curve relationships enables the analysis of structural changes in the US economy that are relevant to monetary policy. The results indicate that the advanced models improve the precision of r-star estimates by responding more effectively to changes in macroeconomic conditions.

keywords: r-star, state-space, Kalman filter, score-driven models

1 Introduction

Due to the unusual magnitude of economic disturbances generated by the Global Financial Crisis (GFC) and the COVID-19 pandemic, potential non-linearities in macro variables have come back into the spotlight. Considering the macroeconomic relevance of the natural rate of interest or r-star and the recent development of the statistical toolkit of time-varying parameter (TVP) models, it is surprising that empirical methodologies employed for its estimation mostly remained unaltered since the seminal work of Laubach and Williams (2003). We fill this gap by making the system matrices in the Laubach-Williams methodology (LW, thereafter) time-varying, based on the score-driven state-space framework developed by Delle Monache et al. (2021). In addition, to address model instability due to extraordinary transitory shocks, we propose an extension of the accelerating generalised autoregressive score model (aGAS) of Blasques et al. (2019), in which the volatility dynamics become fully state-dependent in a multivariate setting.

*Giuseppe Storti acknowledges financial support from the PRIN 2022 grant *Methodological and computational issues in large-scale time series models for economics and finance (20223725WE) - D53D 2300610 0006 - Measure 4-Component 2-Investment 1.1*

The natural rate of interest is an essential macroeconomic benchmark for investors and central banks as it provides an estimate for the real short-term interest rate that keeps the inflation rate constant. Therefore, its vital role lies in its information content about the position of the actual real interest rate compared to its natural counterpart. More specifically, when the actual real rate is above (below) the r-star, the economy operates under (above) its potential level, implying deceleration (acceleration) of the inflation rate. Nevertheless, the natural rate of interest is an unobserved variable, a feature that has motivated various methodological approaches and led to considerable estimation uncertainty since the concept was first proposed by Wicksell (1936).

Recognising the low-frequency and time-varying nature of macroeconomic unobservables made the Kalman filter (Kalman, 1960) the optimal choice for data-driven estimation of latent variables, i.e. Staiger et al. (1996); Gordon (1998), and Laubach (2001). By identifying the natural rate of interest through economic theory in a semi-structural framework, the most prevailing approach to its real-time estimation became the LW methodology, where the Kalman filter extracts the permanent or highly persistent changes in the real short-term interest rate consistent with a stable inflation rate. While the LW framework provides a coherent way to study the unobservable components of the model, the initial study found the r-star estimates to be highly imprecise and prone to substantial real-time measurement error (Laubach and Williams, 2003). Despite the uncertainty around model estimations, the original approach has been applied in numerous studies for different economies and with various extensions (i.e., Garnier and Wilhelmsen, 2009; Holston et al., 2017; Krustev, 2019). However, the global financial crisis (GFC) drew attention to the potential instability in the underlying New Keynesian (NK) structural relationships, casting doubt on the static slope of the model framing IS and Phillips curves. For example, the study of Ball and Mazumder (2011) suggests altering inflation dynamics in the post-GFC interval. Also, Inoue et al. (2022) find a substantial change in the slope of the Phillips curve since 1980. While the related quantitative results are not inclusive and remain without unanimous consensus, most of the studies reject the time-invariant nature of the NK structural relationships.

Concerns about macro non-linearities culminated with the onset of the COVID-19 pandemic. Extremely volatile episodes generated by exogenous events rendered the LW static volatility model less capable of capturing low-frequency changes in the unobservables. As a response, Holston et al. (2023) introduced a macroeconometric adjustment to the existing model, exclusively applied to the interval affected by the pandemic. While the amended model effectively handles the pandemic-related extreme volatility, the implemented restrictions and the ad-hoc nature of the adjustment limit its universal and real-time applicability.

We address the above issues and estimate the r-star in the US by making the disturbance volatilities and the structural relationships in the LW framework time-varying, governed by the conditional score of the likelihood function. The proposed model is an extension of the class of score-driven state-space models introduced by Delle Monache et al. (2021), incorporating a modified version of the accelerating GAS (aGAS) of Blasques et al. (2019). We coin the new type of aGAS as augmented accelerating GAS (aaGAS), where, in addition to the time-varying weight of the conditional likelihood score, the autoregressive coefficient can become time-varying as well, making the volatility dynamics fully state-dependent. To perform a thorough assessment of the estimation uncertainty, we combine the inferential setup of

Blasques et al. (2016), where only parameter uncertainty is considered, with a simulation procedure based on the methodology proposed by Hamilton (1986), which allows us to incorporate the impact of filter uncertainty, an aspect particularly relevant to unobservable component models. The results show that the proposed methodological improvements provide a more effective way to disentangle transitory and permanent shocks, resulting in a more accurate estimation of the state variables. Finally, relying on a purely statistical, data-driven approach, the model is expected to handle and identify unexpected future volatility shocks without the need for major ad hoc econometric adjustments, thus providing a valid alternative empirical approach for the real-time estimation of the natural rate of interest.

The paper is structured as follows. Section 2 presents the econometric framework by first introducing the structure of the time-varying parameter model in Section 2.1, followed by the description of the baseline score-driven state-space model in Section 2.2. In Section 2.3, we extend the framework by introducing an augmented accelerating score-driven approach for time-varying volatility persistences. Section 3 then outlines the empirical analysis, beginning with the data description in Section 3.1, followed by the model specification and estimation details in Section 3.2. The parameter estimates are discussed in Section 3.3 while Section 3.4 and 3.5 report the estimated time-varying volatilities and the dynamic IS and Phillips curves, respectively. Section 3.6 focuses on the estimated state variables by exploring the r-star and the output gap estimates. Finally, Section 4 concludes the paper.

2 The Econometric Framework

2.1 The structure of the time-varying parameter model

In line with the standard LW approach, moving from the classical definition of r-star as the real interest rate consistent with zero output gap and stable inflation, the econometric identification of the natural rate of interest is achieved through two structural relationships associated with the above definition. Specifically, the intertemporal IS dynamics mechanically connect the r-star to the output gap, which, in turn, is closely linked to the inflation rate dictated by the Phillips curve relationship. Accordingly, the following measurement equations drive the model dynamics and provide theoretical support for the econometric identification of the natural rate of interest:

$$\tilde{y}_t = a_1\tilde{y}_{t-1} + a_2\tilde{y}_{t-2} + \frac{a_{\tilde{y},t}}{2}\sum_{j=1}^{2}\left(r_{t-j} - r^*_{t-j}\right) + \varepsilon_{\tilde{y},t} \qquad \varepsilon_{\tilde{y},t} \sim \mathcal{N}(0, \sigma_{\tilde{y},t}) \tag{1}$$

$$\pi_t = b_1\pi_{t-1} + (1-b_1)\pi_{t-2,4} + b_{\pi,t}\tilde{y}_{t-1} + \varepsilon_{\pi,t} \qquad \varepsilon_{\pi,t} \sim \mathcal{N}(0, \sigma_{\pi,t}) \tag{2}$$

where, similar to Holston et al. (2017) (HLW, thereafter), r_t and r^*_t denote the real federal funds rate and its natural level r-star, respectively, π_t is the consumer price inflation rate, $\pi_{t-2,4}$ is the average of the second to fourth lags of the inflation rate. The system of equations (1)-(2) represents the NK intertemporal IS and the Phillips curve relationships based on the HLW specification with a departure for their respective slope parameters, $a_{\tilde{y},t}$ and $b_{\pi,t}$, which become time-varying in the present model. In the IS equation, the output gap series $\tilde{y}_t = 100 \cdot (y_t - y^*_t)$, the percentage difference between the actual (log-transformed) output y_t and its natural level y^*_t, is generated by its lagged values, a moving average of the lagged

r-star adjusted real-funds rate and a Gaussian White Noise (GWN) error. In the Phillips curve equation, the inflation dynamics, π_t, are governed by past inflation rates, the lagged output gap, $\tilde{y}_t$, and a GWN error process.

The presence of the two stochastic terms, $\varepsilon_{\tilde{y},t}$ and $\varepsilon_{\pi,t}$, plays a key role in disentangling transitory shocks from structural persistent shocks which affect the dynamics of the state variables. Moreover, it is well known that changing economic conditions are likely to lead to volatility clustering in the dynamics of macro-variables, such as inflation and output. If not properly modelled, this feature can contaminate the estimates of the state variables and, hence, the structural components of the observed variables. Therefore, we depart from the typical static LW specification with regard to the standard deviations of the disturbances, $\varepsilon_{\tilde{y},t}$ and $\varepsilon_{\pi,t}$, by allowing for time variation in their volatilities, $\sigma_{\tilde{y},t}$ and $\sigma_{\pi,t}$.

We then define r-star based on the HLW specification. According to the neo-classical growth model, the steady-state real one-period interest rate is given by

$$r^* = \frac{1}{\sigma} g_c + \theta$$

where σ represents the intertemporal elasticity of substitution in consumption, g_c denotes the growth rate of per capita consumption, and θ is the rate of time preference. This relationship leads us to the standard monetary DSGE models, where r^* given in Eq. (3) provides an effective method for determining the intercept in the applicable reduced form interest rate rules (i.e., Taylor, 1993).

Given the above theoretical linkage and assuming a unit elasticity of substitution σ as in HLW, the r-star is then determined by

$$r_t^* = g_t + z_t \tag{3}$$

where g_t is the trend growth rate of the natural rate of output and z_t captures other determinants of the natural rate of interest, such as households' rate of time preference.

Having defined the r-star, we finally introduce the system of transition equations governing the dynamics of the latent variables g_t and z_t and of the potential output y_t^* as

$$y_t^* = y_{t-1}^* + g_{t-1} + \varepsilon_{y^*,t} \qquad \varepsilon_{y^*,t} \sim \mathcal{N}(0, \sigma_{y^*,t}), \tag{4}$$

$$z_t = z_{t-1} + \varepsilon_{z,t} \qquad \varepsilon_{z,t} \sim \mathcal{N}(0, \sigma_z), \tag{5}$$

$$g_t = g_{t-1} + \varepsilon_{g,t} \qquad \varepsilon_{g,t} \sim \mathcal{N}(0, \sigma_g). \tag{6}$$

The transition of the potential output, y_t^*, follows a random walk, with a stochastic drift term given by the lagged trend growth rate, g_{t-1}. The variable z_t, which captures any persistent shocks to the r-star that are not captured by g_t, also follows a random walk similar to the trend growth rate. Again, this configuration is comparable to that in HLW, with one important exception being the volatility of the potential output, $\sigma_{y^*,t}$, which is assumed to be time-varying, thus completing the dynamic specification of the time-varying signal-to-noise ratio $\sigma_{y^*,t}^2/\sigma_{\tilde{y},t}^2$. As will be shown later, the signal-to-noise ratio is a central pillar in the identification of persistent shocks in our setting. Accurate identification of its dynamics is expected to improve the performance of the Kalman filter procedure used for inference on the latent state variables.

The parameters that are allowed to evolve in our modelling framework are collected in the time-varying parameter (TVP) vector

$$\lambda_t = (\sigma_{\tilde{y},t}, \sigma_{\pi,t}, \sigma_{y^*,t}, a_{\tilde{y},t}, b_{\pi,t})',$$

where

$$\sigma_{i,t} = \exp\left(\bar{\sigma}_{i,t}\right), \quad i = \{\tilde{y}, \pi, y^*\}, \quad a_{\tilde{y},t} = -\exp(\bar{a}_{\tilde{y},t}), \quad b_{\pi,t} = \exp\left(\bar{b}_{\pi,t}\right).$$

The remaining *static* parameters are included in the vector

$$\theta_s = (a_1, a_2, b_1, \sigma_g, \sigma_z)', \quad \sigma_i = \exp\left(\bar{\sigma}_i\right), \quad i = \{g, z\}.$$

To model the dynamics of the time-varying parameters, we adopt a score-driven approach implying that λ_t is a function of past information available at time $(t-1)$, that is $\lambda_t = \lambda(\mathcal{I}_{t-1})$. The derivation of the score-driven recursions for modelling the dynamics of the elements of λ_t is addressed in the next Section 2.2.

2.2 The baseline score-driven conditionally Gaussian State-Space model

Because of their flexibility, *score-driven* models such as the generalised autoregressive score (GAS) model (Creal et al., 2013) or, referring to the same concept, the dynamic conditional score (DCS) model (Harvey, 2013), have become a popular choice for introducing time-varying parameters in parametric time series models. GAS models can be seen as a class of observation-driven models in which the conditional scaled score of the likelihood function drives the parameter dynamics. The reliance on the full probability density conditional on past information, rather than on specific moments, makes the use of score-driven models particularly attractive.

Leveraging the feasibility of the approach in a multivariate Gaussian setting, Delle Monache et al. (2021) proposed the score-driven state-space model (SSM), where the time variation in the system matrices is modelled following a score-driven approach. An attractive reason for extending the standard linear SSM in a score-driven framework is that it provides a viable strategy for dealing with dynamic parameter restrictions, which are often required by identification based on economic theory. In this respect, the score-driven SSM framework provides a flexible and tractable approach to make the volatilities and NK structural relationships time-varying in the LW framework.

Before introducing the score-based updating mechanism for the time-varying parameters, it is helpful to first cast in matrix state-space form the structural framework described in Section 2.1. Specifically, the corresponding state-space model (Harvey, 1990) is expressed as follows.

$$\mathbf{y}_t = \mathbf{\Gamma}_t \mathbf{u}_t + \mathbf{Z}_t \boldsymbol{\alpha}_t + \boldsymbol{\varepsilon}_t \qquad \varepsilon_t \sim \mathcal{N}(0, \mathbf{H}_t) \tag{7}$$

$$\boldsymbol{\alpha}_t = \mathbf{T}\boldsymbol{\alpha}_{t-1} + \boldsymbol{\eta}_t \qquad \eta_t \sim \mathcal{N}(0, \mathbf{Q}_t) \tag{8}$$

where $\mathbf{y}_t$ is the observation vector collecting the contemporaneous endogenous variables, $\boldsymbol{\alpha}_t$ and $\mathbf{u}_t$ are the vectors of state and input variables, respectively, $\mathbf{T}$ is the state transition matrix, $\mathbf{Z}_t$ is the matrix of regression parameters linking $\mathbf{y}_t$ to the latent states, $\mathbf{\Gamma}_t$ plays the same role for the observed input covariates, $\mathbf{H}_t$ is the variance and covariance matrix of the observation error $\boldsymbol{\varepsilon}_t$, $\mathbf{Q}_t$ is the variance and covariance matrix of the system error $\boldsymbol{\eta}_t$. Formally, the model components and system matrices are defined as follows.

$$\begin{aligned}
\mathbf{y}_t &= \begin{bmatrix} y_t, & \pi_t \end{bmatrix}', \\
\mathbf{u}_t &= \begin{bmatrix} y_{t-1}, & y_{t-2}, & r_{t-1}, & r_{t-2}, & \pi_{t-1}, & \pi_{t-2,4} \end{bmatrix}', \\
\alpha_t &= \begin{bmatrix} y_t^*, & y_{t-1}^*, & y_{t-2}^*, & g_t, & g_{t-1}, & g_{t-2}, & z_t, & z_{t-1}, & z_{t-2} \end{bmatrix}',
\end{aligned}$$

$$\mathbf{Z}_t = \begin{bmatrix} 1 & -a_1 & -a_2 & 0 & -2a_{\tilde{y},t} & -2a_{\tilde{y},t} & 0 & -a_{\tilde{y},t}/2 & -a_{\tilde{y},t}/2 \\ 0 & -b_{\pi,t} & 0 & 0 & 0 & 0 & 0 & 0 & 0 \end{bmatrix},$$

$$\mathbf{\Gamma}_t = \begin{bmatrix} a_1 & a_2 & a_{\tilde{y},t}/2 & a_{\tilde{y},t}/2 & 0 & 0 \\ b_{\pi,t} & 0 & 0 & 0 & b_1 & 1-b_1 \end{bmatrix}, \quad \mathbf{H}_t = \begin{bmatrix} \sigma_{\tilde{y},t} & 0 \\ 0 & \sigma_{\pi,t} \end{bmatrix},$$

$$\mathbf{T} = \begin{bmatrix} 1 & 0 & 0 & 1 & 0 & 0 & 0 & 0 & 0 \\ 1 & 0 & 0 & 0 & 0 & 0 & 0 & 0 & 0 \\ 0 & 1 & 0 & 0 & 0 & 0 & 0 & 0 & 0 \\ 0 & 0 & 0 & 1 & 0 & 0 & 0 & 0 & 0 \\ 0 & 0 & 0 & 1 & 0 & 0 & 0 & 0 & 0 \\ 0 & 0 & 0 & 0 & 1 & 0 & 0 & 0 & 0 \\ 0 & 0 & 0 & 0 & 0 & 0 & 1 & 0 & 0 \\ 0 & 0 & 0 & 0 & 0 & 0 & 1 & 0 & 0 \\ 0 & 0 & 0 & 0 & 0 & 0 & 0 & 1 & 0 \end{bmatrix}, \quad \mathbf{Q_t} = \begin{bmatrix} \sigma_{y^*,t} & 0 & 0 & 0 & 0 & 0 & 0 & 0 & 0 \\ 0 & 0 & 0 & 0 & 0 & 0 & 0 & 0 & 0 \\ 0 & 0 & 0 & 0 & 0 & 0 & 0 & 0 & 0 \\ 0 & 0 & 0 & \sigma_g & 0 & 0 & 0 & 0 & 0 \\ 0 & 0 & 0 & 0 & 0 & 0 & 0 & 0 & 0 \\ 0 & 0 & 0 & 0 & 0 & 0 & 0 & 0 & 0 \\ 0 & 0 & 0 & 0 & 0 & 0 & \sigma_z & 0 & 0 \\ 0 & 0 & 0 & 0 & 0 & 0 & 0 & 0 & 0 \\ 0 & 0 & 0 & 0 & 0 & 0 & 0 & 0 & 0 \end{bmatrix}.$$

It is worth noting again that, unlike HLW, in our framework, the system matrices $\mathbf{Z}_t$, $\mathbf{\Gamma}_t$, $\mathbf{H}_t$ and $\mathbf{Q}_t$ are allowed to be time-varying. Furthermore, without affecting their stochastic nature, the assumed dynamic structure of the vector of time-varying parameters λ_t implies that these matrices are known conditionally on past information $\mathcal{I}_{t-1}$. Therefore, the resulting state-space model, similar to the one introduced by Delle Monache et al. (2021), is conditionally Gaussian, a property that allows us to construct the likelihood function in the usual prediction error decomposition form as in Eq. 9 and use the standard Kalman filter (KF) recursions for optimal state estimation, thus retaining the simplicity of the classical linear Gaussian state space framework. Also, letting the system matrices $\mathbf{Z}_t$, $\mathbf{\Gamma}_t$, $\mathbf{H}_t$ and $\mathbf{Q}_t$ change over time, while still assuming they are non-stochastic given the past, is a practical way to introduce nonlinearities into the state-space model. In fact, assuming that the parameters are determined by past observations, a feature that is compatible with the score-driven methodology, conditional on the past: i) the system variables, observation and state vectors are Gaussian, ii) the observation and transition equations remain linear with respect to the state vector. Nevertheless, these relationships are unconditionally non-linear.

As in the case of time-invariant linear Gaussian state-space models, the model parameters θ are estimated by maximising a Gaussian log-likelihood in its prediction error decomposition form, given by

$$\ell_t = \log p(y_t|\mathcal{I}_{t-1}, \theta) \propto -\frac{1}{2}\left(\log|F_t| + \nu_t' F_{t|t-1}^{-1} \nu_t\right) \tag{9}$$

where the variables involved in the computation of the likelihood function, namely, the prediction error $\nu_{t|t-1}$ and its variance and covariance matrix F_t, along with the conditional mean of the state vector α_t and its mean squared error (MSE) matrix $P_{t|t}$, are estimated recursively in the KF. Formally, the *prediction* equations of the

KF are given by

$$
\begin{aligned}
\alpha_{t|t-1} &= T\alpha_{t-1|t-1} && (\alpha_t|\mathcal{I}_{t-1}) \sim \mathcal{N}(\alpha_{t|t-1}, P_{t|t-1}) \\
P_{t|t-1} &= TP_{t-1|t-1}T' + Q_t \\
y_{t|t-1} &= Z_t\alpha_{t|t-1} + \Gamma_t u_t && (y_t|\mathcal{I}_{t-1}) \sim \mathcal{N}(Z_t\alpha_{t|t-1} + \Gamma_t u_t, F_t) \\
\nu_{t|t-1} &= y_t - y_{t|t-1} \\
F_{t|t-1} &= Z_t P_{t|t-1} Z_t' + H_t
\end{aligned}
$$

while the *filtering* equations are

$$
\begin{aligned}
\alpha_{t|t} &= \alpha_{t|t-1} + K_t\nu_t \\
P_{t|t} &= P_{t|t-1} - K_t Z_t P_{t|t-1} = (I - K_t Z_t)P_{t|t-1} \\
K_t &= P_{t|t-1} Z_t' F_{t|t-1}^{-1}
\end{aligned}
$$

where K_t is known as the *Kalman gain* matrix. As will be demonstrated, the score-driven model allows for high flexibility in updating the elements of the gain matrix, enhancing the ability to allocate the information content embedded in the prediction errors across the state variables. In contrast, in the static-parameter model, these elements converge to a steady-state value with limited time variation, which hampers its efficiency in assigning appropriate weights to the state vector.

Constructing the model in a conditionally Gaussian form facilitates the use of KF to estimate the latent variables. However, it leaves the nontrivial challenge of jointly estimating both the state and the time-varying system matrices, a problem addressed by Delle Monache et al. (2021) using a score-driven approach. The score-driven framework is easily incorporated into the conditional Gaussian state space model by augmenting the KF recursions with a set of additional recursions that track the dynamics of the time-varying coefficients.

Following Creal et al. (2013) and Harvey (2013), the equation for the score-driven updating of the TVP vector λ_t takes the form

$$
\lambda_{t+1} = \omega_\lambda + \mathbf{A}_\lambda \lambda_t + \mathbf{B}_\lambda s_t \quad , \quad s_t = S_{\lambda,t} u_{\lambda,t}, \tag{10}
$$

where

$$
\begin{aligned}
\omega_\lambda &= \left[\omega_{\lambda,\tilde{y}}, \quad \omega_{\lambda,\pi}, \quad \omega_{\lambda,y^*}, \quad 0, \quad 0\right]', \\
\mathbf{A}_\lambda &= \operatorname{diag}\left(\left[\mathrm{a}_{\lambda,\sigma_{\tilde{y}}}, \mathrm{a}_{\lambda,\sigma_\pi}, \mathrm{a}_{\lambda,\sigma_{y^*}}, \mathrm{a}_{\lambda,y^*}, \mathrm{a}_{\lambda,\pi}\right]\right), \\
\mathbf{B}_\lambda &= \operatorname{diag}\left(\left[\mathrm{b}_{\lambda,\sigma_{\tilde{y}}}, \mathrm{b}_{\lambda,\sigma_\pi}, \mathrm{b}_{\lambda,\sigma_{y^*}}, \mathrm{b}_{\lambda,y^*}, \mathrm{b}_{\lambda,\pi}\right]\right).
\end{aligned}
$$

The vector s_t is the gradient of the likelihood function $u_{\lambda,t}$ scaled by the matrix square root of the inverse of the information matrix $S_{\lambda,t}$[1]

$$
u_{\lambda,t} = \frac{\partial \log p(\mathbf{y_t} \mid \lambda_t; \theta)}{\partial \lambda_t} \quad , \quad S_{\lambda,t} = -\mathbf{E_t}\left(\frac{\partial^2 \ell_t}{\partial f_t \partial f_t'}\right)^{-\frac{1}{2}} = \mathcal{I}_t^{-\frac{1}{2}}.
$$

The gradient and the information matrix are computed analytically in parallel with the KF recursion as

$$
u_{\lambda,t} = \frac{1}{2}\dot{F}_t(F_t \otimes F_t)^{-1}\mathrm{vec}(\nu_t\nu_t' - F_t) - 2\dot{V}_t F_t^{-1}\nu_t \tag{11}
$$

[1]To improve numerical stability, we replace $S_{\lambda,t}$ with its smoothed version $\tilde{S}_{\lambda,t} = (1-\kappa)S_{\lambda,t} + \kappa\tilde{S}_{\lambda,t-1}$, where the smoothing parameter κ is estimated jointly with the other model parameters through ML.

$$\mathcal{I}_t = \frac{1}{2}\dot{F}_t(F_t \otimes F_t)^{-1}\dot{F}_t + 2\dot{V}_t F_t^{-1}\dot{V}_t \tag{12}$$

where $\dot{V}_t = \partial\nu_t/\partial\lambda_t$ and $\dot{F}_t = \partial\text{vec}(F_t)/\partial\lambda_t$ measure the sensitivity of the prediction error ν_t and its variance F_t with respect to λ_t. The Jacobian matrices involved in the computation of $\dot{V}_t$ and $\dot{F}_t$ are derived following the approach in Delle Monache et al. (2021). However, it should be noted that, compared to their specification, the observation equation in our model includes an additional regression term, $\mathbf{\Gamma}_t\mathbf{u}_t$. This modification affects the derivation of $\dot{V}_t$, which must be adjusted accordingly to account for the contribution of $\mathbf{\Gamma}_t$. The nonlinear mappings between the TVP vector λ_t and the system matrices, along with the corresponding Jacobians utilised by the score-driven filter, are reported in Appendix B.

In our implementation, in order to limit the proliferation of model parameters, we have assumed the matrices $\mathbf{A}_\lambda$ and $\mathbf{B}_\lambda$ to be diagonal. The diagonal elements of the matrix $\mathbf{B}_\lambda$ ($\text{b}_{\lambda,i}$) determine how sensitive the TVP vector is to the score s_t. Regarding the matrix $\mathbf{A}_\lambda$, its diagonal elements ($\text{a}_{\lambda,i}$) contribute to the degree of persistence of the time-varying parameters by measuring the speed at which the parameter reverts to its long-run level in a shock-free framework. In other words, the diagonal elements of $\mathbf{A}_\lambda$ determine the inertia of the information embedded in the prediction error up to time $t-1$. As discussed in the following section, the above interpretation of the two weighting matrices plays a crucial role in the context of the present study.

Also, since the time variation of the slope parameters is assumed to follow a random walk in the IS and Phillips curve equations, we have imposed $\omega_{\lambda,i} = 0$ and $\text{a}_{\lambda,i} = 1$ in the updating equations for $a_{\tilde{y},t}, b_{\pi,t}$. The vector of static parameters driving the dynamics of the TVP vector λ_t is then given by

$$\boldsymbol{\theta}_\lambda = \{\omega_{\lambda,i}, \mathbf{A}_{\lambda,i}, \mathbf{B}_{\lambda,i}\}, \quad i = \{\sigma_{\tilde{y}}, \sigma_\pi, \sigma_{y^*}, a_{\tilde{y}}, b_\pi\}.$$

The total vector of model parameters to be estimated maximising the log-likelihood in Eq. 9 is $\boldsymbol{\theta} = (\boldsymbol{\theta}_s', \boldsymbol{\theta}_\lambda')'$, which includes the previously introduced vector of static parameters $\boldsymbol{\theta}_s$ and the vector of TVP-related coefficients $\boldsymbol{\theta}_\lambda$.

2.3 An augmented accelerating score-driven framework for TVP updating

The GAS framework allows for score-driven TVPs but relies on the assumption that the dynamic law governing their evolution is time-invariant. However, changing economic conditions and state dependencies, which typically characterise many economic phenomena, can cause the features of the variation pattern to evolve. Furthermore, the flexibility of GAS models is limited by the assumption that the TVPs are linearly dependent on past score values. Blasques et al. (2019) recognised and addressed such difficulties and proposed the accelerating GAS (aGAS) model, which assigns a time-varying weight to the score in the parameter updating equation.

In particular, the aGAS model includes an additional updating equation, where the first-order autocorrelation of the conditional scores determines the weight of the score for updating the dynamic parameters. When recent score innovations have the same sign (positive first-order autocorrelation), the adjustment of the current TVP needs to accelerate faster than in a period when these innovations have mixed signs (negative first-order autocorrelation). Accordingly, the updating procedure will accelerate (decelerate) when a set of consecutive innovations has the

same (different) signs. As a result, the aGAS provides an intuitive way to make the speed of TVP adjustment adaptive, thus improving the local fit of the model. In their analysis, Blasques et al. (2019) find that this mechanism is well suited for capturing sudden volatility shifts, adapting the volatility dynamics much faster than in the standard GARCH model. In addition, they find that in the presence of outliers, the application of the aGAS approach in GARCH-type models can mitigate the adverse effect of tail events by attenuating the impact of the outliers faster.

Considering the above aspects in the present study, the large transitory shocks experienced during the COVID-19 pandemic provide a striking example of rapid shifts in volatility dynamics. As Holston et al. (2023) report, the standardised auxiliary residuals of the output gap display severe divergences from their pre-pandemic level of standard deviation due to the economic shutdowns and re-openings caused by the exogenous shocks. Consistent with a procedure testing the presence of outliers in terms of auxiliary residuals proposed by Harvey and Koopman (1992) and Creal et al. (1999), this observation confirms that the estimated output gap has been heavily affected by the pandemic-induced extreme observations.

Since the main objective in estimating the r-star is to properly disentangle transitory disturbances from permanent or highly persistent shocks using the KF, it is crucial to model volatility persistence adequately. Volatility directly influences the elements of the Kalman gain matrix, which determines the weight assigned to the information content of prediction errors in the state estimation process. As suggested by time series evidence, highly persistent changes in real GDP growth, labour productivity growth, and real interest rate are prone to be mistaken for volatile transitory shocks (Holston et al., 2017). Therefore, maximum likelihood (ML) estimates of the standard deviations in the observation equation are possibly contaminated by persistent changes. As a result, the standard deviations of the state innovations are likely to be biased towards zero when estimated by maximum likelihood, which is the so-called "pile-up problem" mentioned by Stock (1994).

To overcome these problems, we propose implementing an aGAS model, which provides a flexible approach to identifying transitory shocks through adaptive modelling of volatility persistence. As mentioned above, this task is achieved by assigning a time-varying weight to the conditional score. Furthermore, to enhance the flexibility of the aGAS modelling approach, we consider a variant of the model originally proposed by Blasques et al. (2019) where, in the updating mechanism, the autoregressive coefficient associated with the lagged volatility is also allowed to be time-varying. Since this coefficient determines the extent to which current volatility depends on its past values and thus governs its inertia, it plays a prominent role in determining the persistence of volatility clustering over time. This modified version of accelerating GAS will be referred to as augmented accelerating GAS (aaGAS).

In the aaGAS model, the standard score-driven recursion for updating the vector of TVP takes the form

$$\lambda_{t+1} = \omega_\lambda + \mathbf{A}_{\lambda,t}\lambda_t + \mathbf{B}_{\lambda,t}s_t \quad , \quad s_t = S_{\lambda,t}u_{\lambda,t}, \tag{13}$$

where the persistence parameters, given by the diagonal elements of $\mathbf{A}_{\lambda,t}$ ($\mathbf{a}_{\lambda,t}$) and $\mathbf{B}_{\lambda,t}$ ($\mathbf{b}_{\lambda,t}$), become time-varying. The aGAS model is obtained as a special case setting $\mathbf{A}_{\lambda,t} = \mathbf{A}_\lambda$. In our framework, considering the extreme shifts in the volatility of the output gap disturbances during the COVID-19 pandemic, we have decided to enhance the baseline score-driven model presented in Section 2.2 by introducing

an aaGAS update only for the standard deviation of the observation noise in the IS curve equation. To keep the model parsimonious and, therefore, confine the dimension of the TVP-related static parameter vector, the weight parameters associated with the other elements of the TVP vector remain time-invariant, leading to the following modified configuration for the $\mathbf{A}_{\lambda,t}$ and $\mathbf{B}_{\lambda,t}$ matrices in Eq. (13)

$$\mathbf{A}_{\lambda,t} = \text{diag}\left(\left[\boxed{\mathrm{a}_{\lambda,\sigma_{\tilde{y}},t}},\ \mathrm{a}_{\lambda,\sigma_\pi},\ \mathrm{a}_{\lambda,\sigma_{y^*}},\ \mathrm{a}_{\lambda,y^*},\ \mathrm{a}_{\lambda,\pi}\right]\right)$$
$$\mathbf{B}_{\lambda,t} = \text{diag}\left(\left[\boxed{\mathrm{b}_{\lambda,\sigma_{\tilde{y}},t}},\ \mathrm{b}_{\lambda,\sigma_\pi},\ \mathrm{b}_{\lambda,\sigma_{y^*}},\ \mathrm{b}_{\lambda,y^*},\ \mathrm{b}_{\lambda,\pi}\right]\right)$$

where the variation in $\mathrm{a}_{\lambda,\sigma_{\tilde{y}},t}$ and $\mathrm{b}_{\lambda,\sigma_{\tilde{y}},t}$ (boxed) is modelled by the aaGAS specification. For simplicity, we will hereafter denote these as $\mathrm{a}_{\lambda,t}$ and $\mathrm{b}_{\lambda,t}$, respectively.

In particular, following Blasques et al. (2019), the weighting for the i-th component of the score innovation is accomplished as

$$b_{\lambda,t} = j(f_{t+1};\theta) \quad , \quad f_{t+1} = \omega_f + \mathrm{a}_f f_t + \mathrm{b}_f s_{f,t} \tag{14}$$

where $j(\cdot)$ denotes a logistic function that characterises how the additional updating equation governs the time variation in $\mathrm{b}_{\lambda,t}$. The time-varying f_{t+1} follows a first-order autoregressive process with intercept ω_f, AR coefficient a_f, weight parameter b_f, and innovation term $s_{f,t}$, which is given by

$$s_{f,t} = C_{f,t} u_{f,t} \quad , \quad u_{f,t} = \frac{\partial \log p(y_t \mid \lambda_t;\theta)}{\partial f_t} \propto u_{\lambda,t} u_{\lambda,t-1}, \tag{15}$$

where $C_{f,t}$ is a function of the scaling factors $S_{\lambda,t}$ and $S_{\lambda,t-1}$ introduced earlier.

More precisely, since the aaGAS update is applied exclusively to the first element of the TVP vector, we consider only the first diagonal element of the scaling matrices $S_{\lambda,t}$ and $S_{\lambda,t-1}$, such that:

$$C_{f,t} = [S_{\lambda,t}]_{11} \cdot [S_{\lambda,t-1}]_{11},$$

where

$$[S_{\lambda,t}]_{11} = ([\mathcal{I}_t]_{11})^{-\frac{1}{2}}$$

denotes the square root of the inverse of the first diagonal element of the time t information matrix. This scalar scaling term ensures that only the uncertainty related to the output gap volatility enters the aaGAS update so that the current and lagged scores are scaled by their corresponding marginal Fisher information.

To complete the local dependence model of volatility persistence in Eq. (13), we introduce $\mathrm{a}_{\lambda,t}$ given as

$$\mathrm{a}_{\lambda,t} = k(g_{t+1};\theta) \quad , \quad g_{t+1} = \omega_g + \mathrm{a}_g g_t + \mathrm{b}_g s_{g,t} \quad , \quad s_{g,t} = [S_{\lambda,t}]_{11} \cdot u_{g,t}, \tag{16}$$

where the link function and the structure of the updating equation are analogous to Eq. (14), with the innovation term $u_{g,t}$, as shown in Appendix A under the assumption $\partial\lambda_{t-1}/\partial f_t = 0$, defined as

$$u_{g,t} = \frac{\partial \log p(y_t \mid \lambda_t;\theta)}{\partial g_t} \propto u_{\lambda,t}\lambda_{t-1}. \tag{17}$$

Therefore, Eq. (17) reveals that when the weighting coefficient in the score-driven updating equation becomes time-varying, it is proportional to the product

of the current conditional score and the lagged realisation of the time-varying parameter itself, thus relating to the first-order cross-correlation between these variables. One may interpret this result within the present context as follows: a sharp change in the conditional score materialised by a large shock, such as an event associated with the COVID-19 pandemic, implies a sudden downward shift in the volatility persistence. Therefore, the model is expected to identify large transitory shocks more effectively by putting less weight on the AR coefficient of the parameter updating equation.

3 Empirical analysis

This section presents the results of an empirical application of the models introduced in Section 2 to US data. First, Section 3.1 and Section 3.2 provide brief descriptions of the dataset used for the analysis and the estimation strategy, respectively, while Section 3.3 presents the estimation results, Section 3.4 focuses on the estimated time-varying volatilities, the estimated dynamic IS and Phillips curves are presented in Section 3.5, and finally Section 3.6 reports and discusses the empirical results on the estimation of the r-star and the output gap.

3.1 The data

The dataset used in this study is the same as that in Holston (2017), but has been extended to cover the period up to 2024 Q4. Therefore, for a brief overview, we report only the summary of the variables in Table 1. A detailed description of the variables can be found in the Data Appendix of HLW. Further details and the quarterly updated database are available on the website of the Federal Reserve Bank of New York (`https://www.newyorkfed.org/research/policy/rstar`).

Table 1: Variable Definitions

Variable	**Description**
Inflation	Annualised quarterly growth rate of core PCE inflation
Inflation expectations	Four quarter moving average of past inflation
Short-term interest rate	Annualised nominal federal funds rate
Output	Logarithm of real GDP

3.2 Model specification and estimation

We estimate two variants of the baseline TVP conditionally Gaussian state-space model, each employing a different score-driven framework to govern the dynamics of the TVP vector. First, we estimate the model with the standard GAS updating structure; then, we consider the model incorporating the augmented accelerating scheme (aaGAS) for the volatility of the output gap innovations. The model log-likelihood in Eq. 9 is evaluated by the KF, augmented with the score-driven recursions needed to update the time-varying parameters present in the system matrices. Estimation of the vector of model parameters θ, including those kept time-invariant within the system matrices (θ_s) and the TVP-related ones (θ_λ), is carried out by numerically maximising the log-likelihood function with respect to $\theta = (\theta_s, \theta_\lambda)$.

Confidence intervals for the elements of the TVP vector λ_t and the state estimates are constructed by integrating the simulation-based inferential techniques of Blasques et al. (2016) and Hamilton (1986) to account for both parameter and filter uncertainty. More specifically, in addition to generating parameter vectors from a multivariate normal distribution, with mean and variance-covariance matrix respectively given by the ML estimate of the static parameter vector $\hat{\theta}$ and its robust variance-covariance matrix estimate, we simultaneously draw model-based random trajectories of the state vector. As prior for the initial state, we assume a multivariate normal distribution with the mean and variance-covariance matrix given by the smoothed estimates of the initial state and its variance-covariance matrix, respectively. Therefore, the confidence intervals constructed from the simulated sequences of parameter and state vectors obtained using the Kalman filter with the TVP updating algorithm capture both filtering and parameter estimation uncertainty. In addition, to assess the overall precision of the state variable estimates and facilitate comparison with the HLW model, we compute their associated standard errors following the methodology introduced by Hamilton (1986). In what follows, we report standard errors and the 68% confidence intervals based on 5000 simulations.

3.3 Parameter estimates

Before turning to the visual representation of the estimated dynamic parameters and state variables, Table 2 presents a first summary of the estimation results. In addition to the score-driven models, the table also reports the estimation results for the COVID-adjusted version of the benchmark HLW model discussed by Holston et al. (2023). All models consider the period from 1960 Q1 to 2024 Q4, covering the full data set available at the time of writing.

The top panel of the table reports the parameter estimates for the static parameters in θ_s, $(a_1, a_2, b_1, \sigma_g, \sigma_z)$, along with their robust standard errors. For both score-driven specifications, the estimated values are broadly in line with the HLW estimates, except for the standard deviations of the trend growth rate and the z-factor innovations, σ_g and σ_z, which are estimated to be lower under the score-driven models. At this point, it is worth noting that we slightly depart from the related HLW procedure, where the Stock and Watson (1998) median unbiased estimator (MUE) is used due to the pile-up problem discussed in Section 2.3. Our choice aligns with Buncic (2024), who estimates σ_g and σ_z with ML and finds little evidence for the pile-up problem. As the estimated parameters suggest, this finding is also supported by our ML estimates, probably due to the improved identification of transitory shocks facilitated by time-varying volatilities. Concerning the estimation of the TVP vector, in order to enable the comparison with HLW, we summarise the elements of λ_t in terms of their sample averages in the bottom panel of the table. Specifically, we find that the mean values of $\sigma_{\tilde{y}}$, σ_π and σ_{y^*} are consistent with the corresponding HLW estimates. Regarding the two slope parameters, $a_{\tilde{y}}$ and b_π, the former, associated with the IS curve, is well aligned with the HLW estimate. In contrast, the sample average of the latter, corresponding to the Phillips curve, is half the value reported by HLW when using the GAS specifications.[2]

Turning to the assessment of uncertainty in the state variables, the lower panel

[2]The slope parameter of the Phillips curve estimated under the original LW configuration is closer to the sample average of our estimates, i.e., 0.047 over the same estimation interval.

Table 2: Model estimation results

Parameter	**HLW**	**standard GAS**	**aaGAS**
Static $[\theta_s]$			
a_1	1.417	1.514	1.544
	[0.103]	[0.097]	[0.027]
a_2	-0.483	-0.545	-0.578
	[0.105]	[0.084]	[0.035]
b_1	0.689	0.617	0.618
	[0.041]	[0.079]	[0.074]
σ_g	0.137	0.128	0.080
		[0.005]	[0.001]
σ_z	0.113	0.056	0.045
		[0.022]	[0.001]
$\sigma_{r^*} = \sqrt{\sigma_g^2 + \sigma_z^2}$	0.188	0.139	0.092
Time Varying $[\lambda_t]$			
$a_{\tilde{y}}$	-0.068	-0.054	-0.057
	[0.017]		
b_π	0.080	0.040	0.040
	[0.026]		
$\sigma_{\tilde{y}}$	0.437	0.386	0.391
	[0.094]		
σ_π	0.791	0.753	0.739
	[0.027]		
σ_{y^*}	0.503	0.511	0.515
	[0.077]		
S.E. (sample averages)			
r^*	1.207	0.760	0.700
g	0.407	0.400	0.309
y^*	1.520	2.023	1.809
z	1.137	0.644	0.627
S.E. (final observations)			
r^*	1.595	1.073	0.910
g	0.583	0.642	0.452
y^*	2.090	2.878	2.084
z	1.484	0.860	0.789
Log-Likelihood	-600.70	-570.44	-565.81
AIC	1235.4	1174.89	1173.62

Note: Robust standard errors (S.E.) are reported in parentheses. σ_g is expressed at an annual rate. The values for the time-varying counterparts of $\sigma_{\tilde{y}}$, σ_π, σ_{y^*}, $a_{\tilde{y}}$ and b_π under the GAS and aaGAS model correspond to their sample averages. Standard errors for σ_g and σ_z under the HLW model are not reported, as these are implied parameters. Specifically, they are computed as $\sigma_g = \lambda_g \sigma_{y^*}$ and $\sigma_z = \frac{\lambda_z \sigma_{\tilde{y}}}{a_{\tilde{y}}}$, where λ_g and λ_z are obtained from a preliminary ML estimation.

of Table 2 compares the standard errors obtained across the models under consideration. Focusing first on potential output, the sample average standard errors in the GAS models are higher than in the HLW model, indicating somewhat greater estimation uncertainty on average. However, the difference is only marginal in the aaGAS model. As for the final observation, while a similar degree of difference remains in the standard GAS model, the aaGAS model yields a nearly identical

standard error, suggesting that it is not the onset of the COVID-19 pandemic which drives the full-sample divergence from the HLW model in the potential output estimation uncertainty.[3] Most importantly, the sample average standard error of the r-star in the aaGAS model is 0.7 percentage points, which is nearly half the magnitude observed in the HLW model, highlighting a substantial reduction in uncertainty of the natural rate estimate when the full information set is utilised. A comparable gain in precision is also evident in the standard errors of the final observation, reflecting lower uncertainty in the real-time state estimates of the score-driven models. It should be noted that the random walk component, z, accounts for the largest improvement in the precision of r-star estimates and is the main contributor to the estimation uncertainty of the natural rate of interest reported under all models and for both the sample average and final observation estimates.[4]

Overall, the log-likelihood and the information criteria values confirm that the score-driven framework significantly improves the model fit, where the aaGAS model slightly outperforms the standard GAS model.

The additional static parameters governing the score-driven updates, collected in the vector θ_λ, are reported in Table 3. Most parameters are significant at the 10% level in both score-driven models. The most notable exception is given by the score weight associated with the output gap standard deviation, $\mathrm{b}_{\lambda,\sigma_{\tilde{y}}}$, indicating some uncertainty in the identification of the dynamics of the underlying coefficient in the standard GAS model. As $\mathrm{a}_{\lambda,\sigma_{\tilde{y}}}$ and $\mathrm{b}_{\lambda,\sigma_{\tilde{y}}}$ are modelled as time-varying in the aaGAS framework, we report the time averages of the estimated coefficients to allow comparison with the level of the corresponding GAS estimates.

3.4 Time-varying volatilities

In this section, we compare the estimates of time-varying volatilities obtained by the GAS and aaGAS approaches.

First, Figure 1 shows the evolution of the parameters governing the state-dependent persistence of the output-gap volatility within the aaGAS setting. The time-varying AR coefficient $\mathrm{a}_{\lambda,t}$ exhibits large movements during the analysed period. Notably, the dynamics of $\mathrm{a}_{\lambda,t}$ appear to be correlated with those of the output as the sharp declines in the coefficient coincide with the US recessionary periods characterised by plummeting US output. In general, it can be observed that $\mathrm{a}_{\lambda,t}$ decreases proportionally to the magnitude of output shocks. These drops are regularly followed by a slow recovery as economic disruptions dissipate. This behaviour is particularly pronounced during the COVID-19 pandemic, reflecting highly volatile economic activity. During the same period, the parameter $\mathrm{b}_{\lambda,t}$, which measures the weight of score innovations, is characterised by a sharp increase after an initial decrease. This variation enables a quicker adjustment to the new level of volatility. Consequently, the lower level of $\mathrm{a}_{\lambda,t}$ implies that the overall persistence of the output gap during the COVID period is predominantly driven by the score innovations rather than by the inertial component of its dynamics.

[3] We find that the standard errors of potential output generated by the aaGAS model are, on average, similar to those obtained from the original Laubach and Williams (2003) model configuration with the COVID-related modification introduced by Holston et al. (2023), and lower for the final observation, which reports 1.8 and 2.5 percentage points, respectively.

[4] We note that the gains in the estimation precision are similar or even greater when comparing the standard errors of the r-star and its components obtained by our models with those by the Laubach and Williams (2003) specification.

Table 3: TVP Related Parameter Estimates

Parameter	**standard GAS**	**aaGAS**	**Parameter**	**aaGAS**
$a_{\lambda,\sigma_{\tilde{y}}}$	0.826	0.463	$a_{f,\sigma_{\tilde{y}}}$	0.837
	[0.053]			[0.016]
$a_{\lambda,\sigma_{\pi}}$	0.900	0.898	$b_{f,\sigma_{\tilde{y}}}$	0.006
	[0.050]	[0.042]		[0.002]
$a_{\lambda,\sigma_{y^*}}$	0.838	0.740	$\omega_{f,\sigma_{\tilde{y}}}$	0.490
	[0.145]	[0.009]		[0.005]
$b_{\lambda,\sigma_{\tilde{y}}}$	0.498	0.440	$a_{g,\sigma_{\tilde{y}}}$	0.845
	[0.268]			[0.026]
$b_{\lambda,\sigma_{\pi}}$	0.142	0.139	$b_{g,\sigma_{\tilde{y}}}$	0.030
	[0.032]	[0.031]		[0.001]
$b_{\lambda,\sigma_{y^*}}$	0.275	0.221	$\omega_{g,\sigma_{\tilde{y}}}$	0.464
	[0.096]	[0.011]		[0.074]
$b_{\lambda,\tilde{y}}$	0.118	0.078		
	[0.116]	[0.016]		
$b_{\lambda,\pi}$	0.006	0.003		
	[0.008]	[0.004]		
$\omega_{\lambda,\sigma_{\tilde{y}}}$	0.719	0.366		
	[0.345]	[0.047]		
$\omega_{\lambda,\sigma_{\pi}}$	0.945	0.940		
	[0.036]	[0.027]		
$\omega_{\lambda,\sigma_{y^*}}$	0.804	0.708		
	[0.368]	[0.013]		
κ	0.014	0.036		
	[0.007]	[0.004]		

Note: Robust standard errors are reported in parentheses. The values for the time-varying counterpart of $a_{\lambda,\sigma_{\tilde{y}}}$ and $b_{\lambda,\sigma_{\tilde{y}}}$ under the aaGAS model correspond to their sample averages.

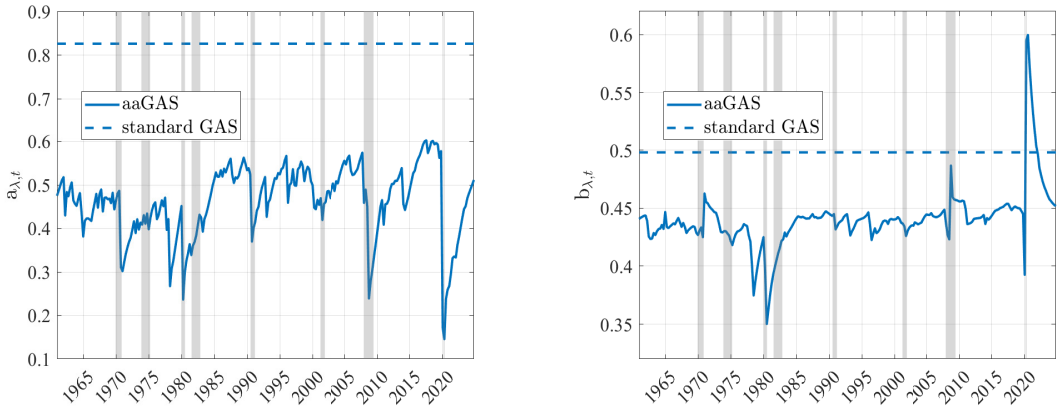

Figure 1: Dynamic persistence parameters of the output gap noise volatility estimated by the aaGAS (solid line) and standard GAS (dashed line) specifications. The left-hand side panel displays the inertia coefficient $a_{\lambda,t}$, the right-hand side panel shows the weight of the score innovations $b_{\lambda,t}$.

Next, Figures 2 and 3 show the time plots of the output gap and potential output volatilities, respectively, comparing the time-varying volatility dynamics returned by the score-driven models (GAS and aaGAS) with the volatility level fitted by

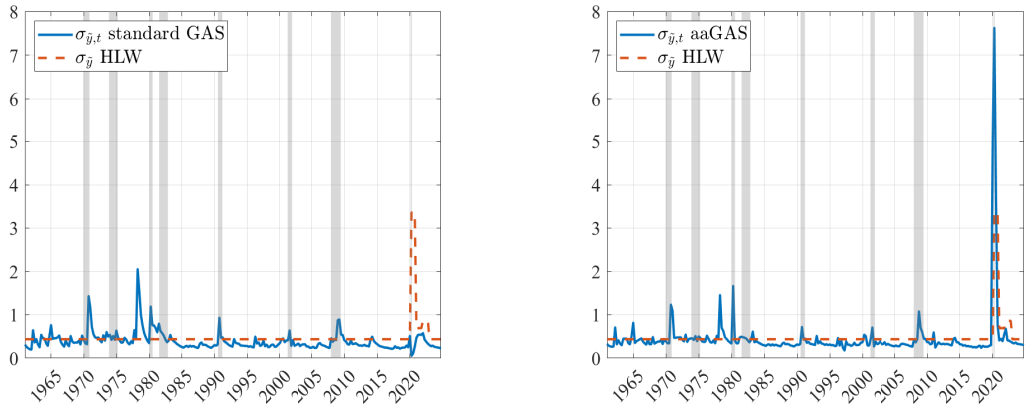

Figure 2: The solid blue lines show the output gap time-varying volatilities estimated by the standard GAS (left) and augmented-accelerating GAS update (right). The red dashed lines display the HLW estimates adjusted in the COVID-19 pandemic by the HLW (2023) methodology. Shaded vertical areas indicate US recessions as dated by the National Bureau of Economic Research (NBER).

the COVID-adjusted HLW model. The latter assumes a constant volatility level except for the ad hoc adjustment characterising the COVID-19 period.

For the output gap, as shown in Figure 2, the aaGAS and GAS approaches produce volatility patterns that differ substantially during the COVID-19 pandemic. While the standard GAS specification does not capture the shock induced by pandemic restrictions, the aaGAS model estimates notably higher volatility, consistent with the definition of a transitory shock. Over the long run, the HLW constant estimate interpolates the score-driven volatilities while, during the COVID period, it lies between the GAS and aaGAS estimates.

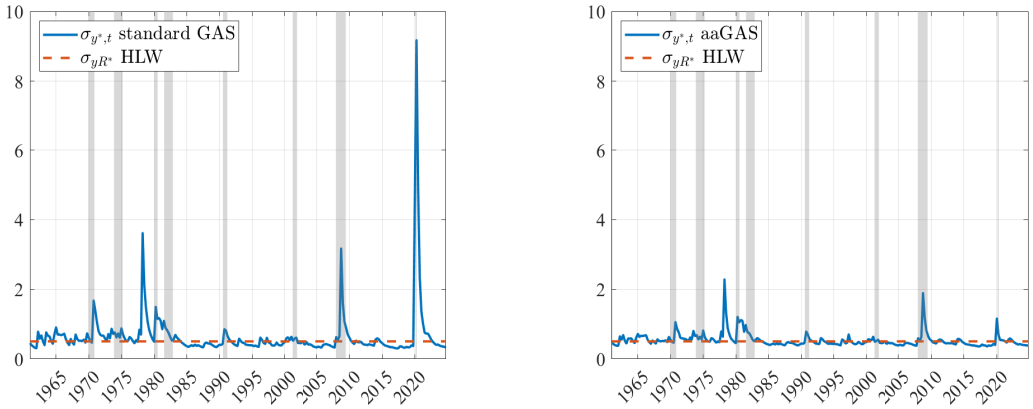

Figure 3: Potential output time-varying volatilities estimated by the standard GAS (left) and augmented-accelerating GAS update (right). The red dashed lines show the time-invariant counterparts estimated by HLW. Shaded vertical areas indicate U.S. recessions as dated by the National Bureau of Economic Research (NBER).

Introducing fully state-dependent persistence in output gap volatility does not limit its impact to a single parameter. This is evident in Figure 3, which shows the difference between the conditional volatility estimates of potential output obtained from the two score-driven models. While the standard GAS update allows the pandemic-related innovations to affect the signal, the aaGAS updating mechanism mitigates the impact of these shocks on state volatility by downweighting the associated scores through Eq. 11 and Eq. 12. This behaviour is better understood

when considering that the pandemic-specific trajectories in the volatility dynamics result in a different evolution of the signal-to-noise ratio - that is, the ratio of output gap to potential output volatility - a critical factor in estimating the state through the KF. As shown in the bottom panel on the left-hand side of Figure 4, when the model is estimated by the standard GAS model, the ratio rises sharply due to the COVID-19 pandemic shocks, considerably affecting the path of the potential output. In contrast, as will be shown in Section 3.6, the aaGAS model discounts the weights on the same shocks in the KF through the signal-to-noise ratio (bottom panel on the right-hand side of Figure 4), thus minimising the impact of transitory shocks on the state variable and leaving the potential output nearly unaffected. In addition, the bottom-right panel shows that, while the estimated trajectories obtained from the aaGAS and the HLW estimates follow a broadly similar pattern, their timing differs slightly when compared. It should be noted that the delayed response of the latter results from a COVID-related modelling choice by Holston et al. (2023), which allows the underlying output gap volatility to vary annually, but only starting in the second quarter of 2020, despite the U.S. economy having already been affected by the COVID shock in the first quarter of 2020.

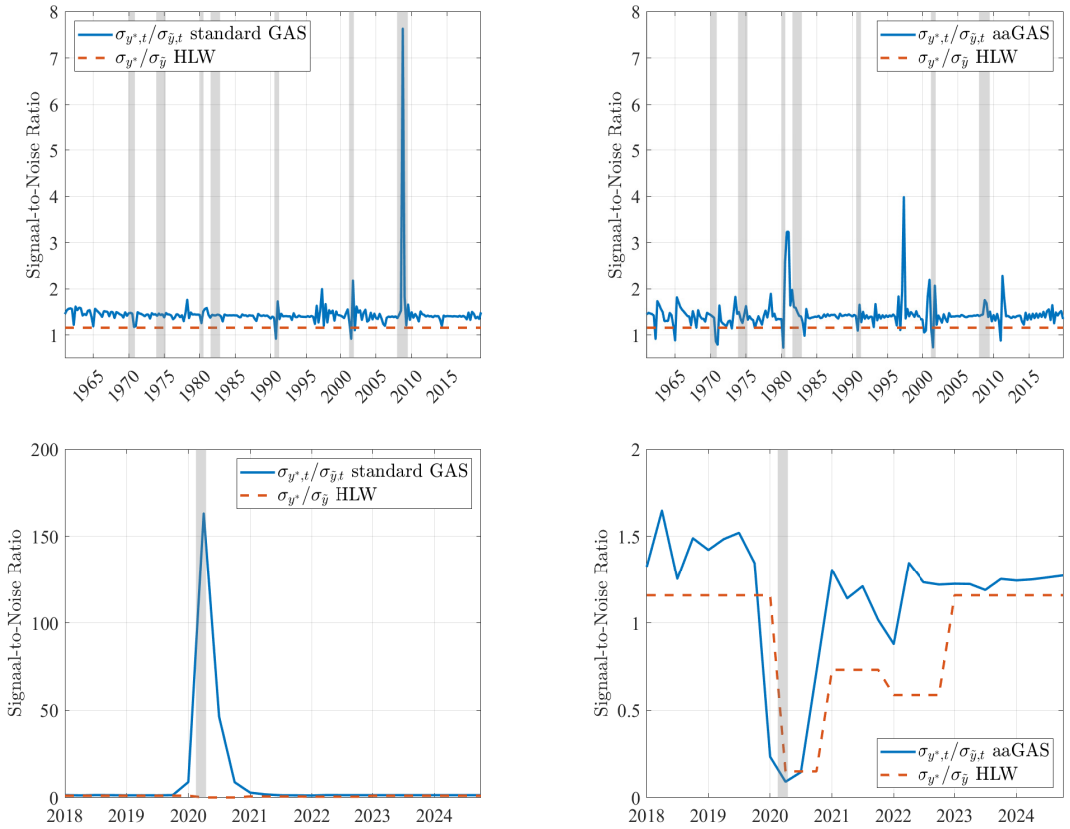

Figure 4: The solid blue lines show the signal-to-noise ratio (output gap volatility to potential output volatility) estimated by the standard GAS (left-hand side column) and augmented-accelerating GAS update (right-hand side column) in the pre-pandemic interval (upper panels) and from 2018 onward (bottom panels). The red dashed lines display the HLW estimates adjusted in the COVID-19 pandemic by the HLW (2023) methodology. Shaded vertical areas indicate U.S. recessions as dated by the National Bureau of Economic Research (NBER).

To conclude the section, Figure 5 depicts the volatility dynamics of the inflation, which agrees with the major inflationary events.[5] The 1970s hikes align with the

[5]Since the estimation of this time-varying parameter largely coincides in the two models, only

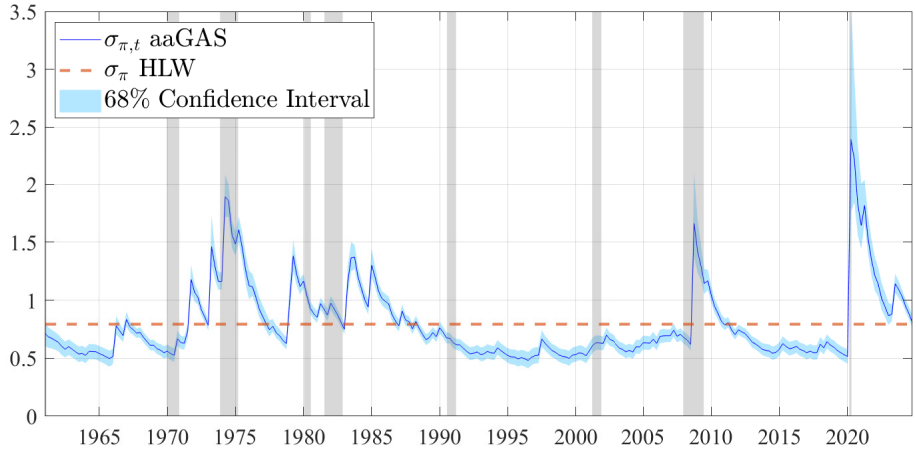

Figure 5: Inflation volatility estimated by the aaGAS model. The coloured bands denote the 68% confidence interval corresponding both for filtering and parameter uncertainty. The red dashed lines show the time-invariant inflation volatility estimated by HLW (2017). Shaded vertical areas indicate U.S. recessions as dated by the National Bureau of Economic Research (NBER).

oil shocks and energy crisis, setting off a trend of high inflation in the US. It was not until the middle of the 1980s that the high inflation volatilities petered out, due to the Volcker monetary tightening. This period of low volatility, known as the 'Great Moderation', came to an end with the GFC, when the standard deviation of inflation increased sharply. Lastly, the COVID-19 pandemic-induced inflationary shocks, followed by the disruption in the energy market in 2023, are also reflected in the evolution of the Phillips curve-related standard deviation.

3.5 Dynamic IS and Phillips curves

This section evaluates the dynamics of the parameters that drive the IS and Phillips curve structural relationships. As the evolution of the two time-varying parameters in the two score-driven models considered takes a comparable path, only the results obtained by estimating the aaGAS model are reported.

Figure 6 displays the dynamics of the IS and Phillips curve slope parameters over the analysed interval, respectively. Specifically, $a_{\tilde{y},t}$ corresponds to the output gap sensitivity to changes in the real interest rate gap, and $b_{\pi,t}$ determines the linkage between the output gap and the inflation rate. While a causal interpretation of the endogenous relationships requires the identification of the individual structural shocks, the main linkages can be summarised as follows. When the real funds rate is above (below) the natural rate of interest, the positive (negative) real rate gap reduces (increases) economic activity. The resulting lower (higher) output gap is, in turn, associated with deflationary (inflationary) conditions.

The evolution of the IS slope parameter in the left-hand side panel confirms that the relationship between the real interest rate gap and the output gap underwent considerable structural changes over the analysed interval. Specifically, until the economic recovery from the 1990s recession, the IS slope appears unstable and relatively steep. However, in line with the unfolding Great Moderation, characterised by downward shifts in economic volatility and consolidating monetary policy, the

the aaGAS estimates are presented.

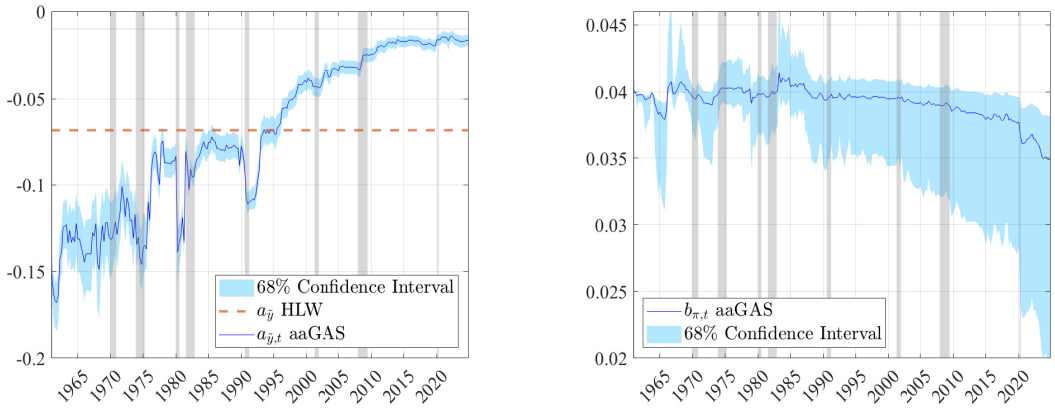

Figure 6: Dynamic slopes of the IS curve (left-hand side) and Phillips curve (right-hand side) based on simulation output. The red dashed line shows the time-invariant slope of the IS curve estimated by HLW (2017). The Phillips curve slope parameter estimated by HLW (2017) as 0.08 is not displayed to improve readability. The solid blue line corresponds to the 50th percentile of the simulated parameter. Shaded vertical areas indicate U.S. recessions as dated by the National Bureau of Economic Research (NBER).

slope gradually became flatter, reaching its current relatively stabilised level after the Great Recession.

Although the Phillips curve slope dynamics in the right-hand side panel follow a downward trend, the median of the simulated parameter path remains confined to a narrow range due to the low weight placed on its score innovation, $b_{\lambda,\pi}$, as reported in Table 3. This finding suggests that the relationship between the output gap and the inflation rate has been relatively stable in the analysed interval, consistent with studies reporting small or no significant change in the slope of the Phillips curve in recent decades (i.e., Hazell et al., 2022). Nevertheless, the asymmetrical widening of the confidence bands over the last two decades makes it difficult to rule out the flattening Phillips curve hypothesis.

3.6 The r-star and the output gap

To open the discussion, we compare the output gap dynamics around the COVID pandemic obtained by the two GAS specifications discussed in Section 3.4 with those implied by the HLW estimates. As Figure 7 illustrates, the output gap filtered state trajectories under the two score-driven models diverge markedly from the onset of the COVID-19 pandemic. Interestingly, from this point onward, the median realisation of the simulated state under the standard GAS model deviates from its filtered counterpart, resulting in more comparable simulated paths across the considered models. However, consistently with the significance of the weighting parameters related to the standard deviation of the output gap reported in Table 3, the narrower confidence band, with the closer alignment between the simulated and filtered states, under the aaGAS model suggest that introducing time-varying persistence in output gap volatility substantially improves both the precision and the real-time reliability of the estimates.

While the aaGAS output gap exhibits the expected behaviour as the COVID-19 pandemic evolves, the decline in its magnitude differs markedly from that estimated by HLW. Figure 8 presents the distinct estimates of the underlying states that, by definition, give rise to the observed dynamics. Notably, the natural rate of output moderately declines in all considered models following the initial impact

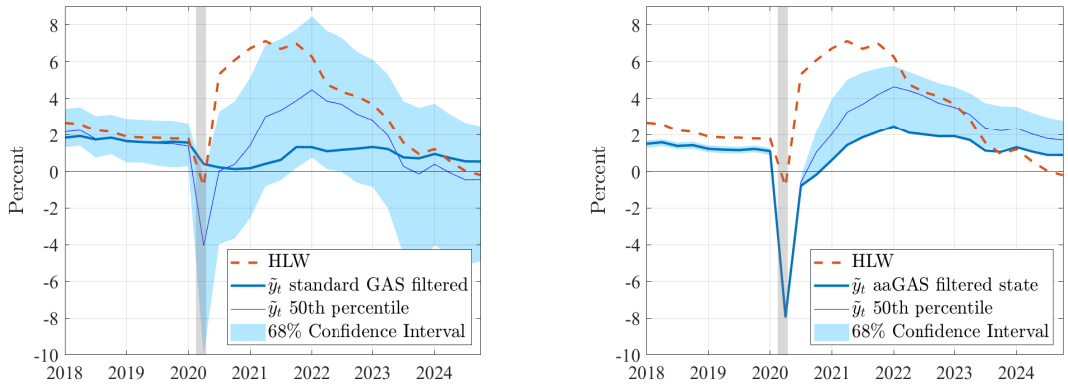

Figure 7: Estimations of the output gap around the COVID pandemic using the model with standard GAS (left-hand side) and augmented-accelerating GAS (aaGAS) update (right-hand side). The coloured bands denote the 68% confidence interval accounting for both filtering and parameter uncertainty. The thin solid blue line indicates the 50th percentile of the simulated states, while the thick blue line shows the real-time filtered estimates. Shaded vertical areas indicate U.S. recessions as dated by the National Bureau of Economic Research (NBER).

of the pandemic, but diverges noticeably thereafter. While the y-star estimated by the standard GAS and HLW models falls more sharply in 2020 Q2, the former rebounds significantly, whereas the latter continues along a shifted trend as the economic impact of the pandemic unfolds. In contrast, the aaGAS model interprets the pandemic-related shocks as transitory, resulting in a potential output estimate that follows a moderately shifted trend with a milder slope. Given the primary objective of the Kalman filter in this study, the substantial shift in the standard GAS and HLW state estimate appears difficult to reconcile with the typically persistent nature of potential output. In contrast, the aaGAS scenario, which shows a trend with a moderate downward shift, with increased uncertainty around the output gap, aligns more closely with the somewhat neutralising forces on productivity experienced after the initial shock of the COVID-19 pandemic.[6]

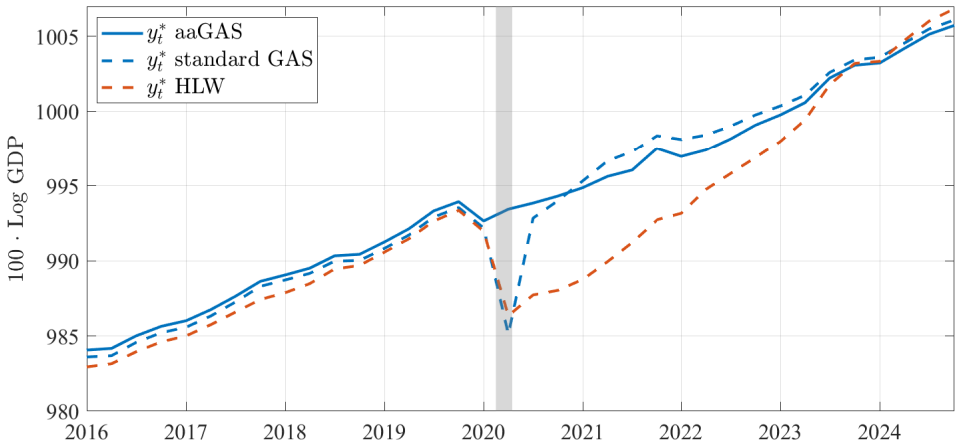

Figure 8: Estimation of the potential output by different models around the COVID-19 pandemic.

[6]For example, Bloom et al. (2025) find little lasting impact on aggregate total factor productivity with significant heterogeneity across firms and sectors in the US. Similarly, Fernald and Li (2022) report a relatively modest decline in potential output in the post-COVID interval, driven by offsetting effects across different channels.

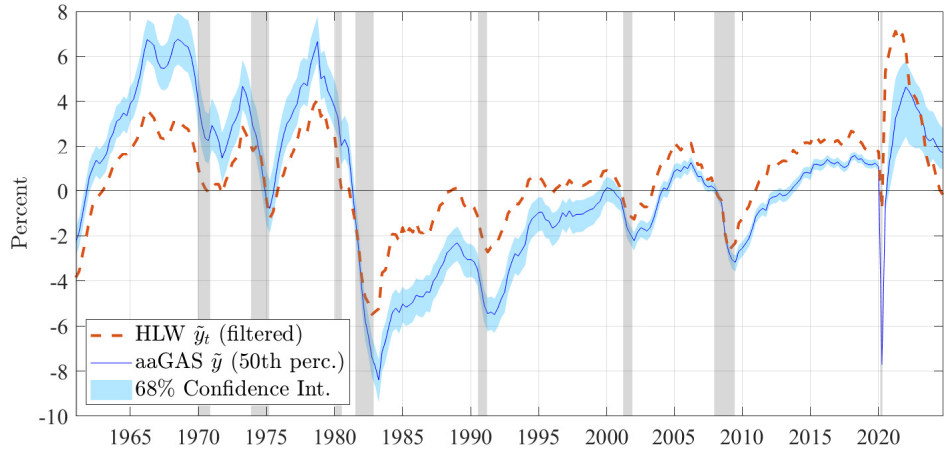

Figure 9: Output gap 50th percentile simulation projection by the aaGAS model with the corresponding confidence band and the benchmark HLW filtered estimate. Shaded vertical areas indicate U.S. recessions as dated by the National Bureau of Economic Research (NBER).

Looking at the output gap over the full interval, Figure 9 reveals that the declines in output gap at the aaGAS model are generally deeper than the HLW estimations. The fall in the output gap is especially pronounced following the Volcker shock, which proceeds with a slower rebound than the HLW estimation. This mismatch arises from the higher potential output the score-driven model gives, likely reflecting its muted sensitivity to transitory shocks consistent with the structural assumption. These characteristics suggest that models with time-varying volatilities improve the effectiveness of filtering out temporary disturbances when estimating state variables. In addition, the resulting asymmetry, which, except for the high-inflation trend episodes in the 1960s and 1970s and the post-COVID period, dominates the analysed interval, is somewhat compatible with the "plucking model" by Friedman (1993), where the economy fluctuates under its full potential ceiling.[7]

Turning to the central interest of the study, Figure 10 displays the r-star estimated by the aaGAS specification with a confidence interval accounting for both parameter and filtering uncertainty.[8] As the plot displays, the natural rate of interest follows a descending trend through the analysed interval and, as shown in Figure 11, its real-time estimate is characterised by a relatively lower variability than the corresponding HLW estimate. Most importantly, the decline during the GFC is less pronounced in our estimation and, even afterwards, tends to stay in a higher range than the HLW estimate. The distinct trajectory of the aaGAS r-star, as shown by the two-sided estimates in Figure 11, becomes even more evident when comparing its smoothed values given by the KF recursion using the full information set. Nevertheless, considering the ongoing debate about the current location of the r-star, the most intriguing finding is perhaps the observed divergence in the trends of the two real-time estimates.

As Figure 12 shows, the primary source of the estimation discrepancy is the fundamentally different paths of the "other factors" component, z_t. While the descent in z_t estimated by HLW accelerates in the post-pandemic interval, it shows

[7]The plucking framework has been studied recently both theoretically (Suah, 2024) and empirically (Dupraz et al., 2019).

[8]Except for the potential output, we report only the state estimations of aaGAS as these results are robust over the two specifications.

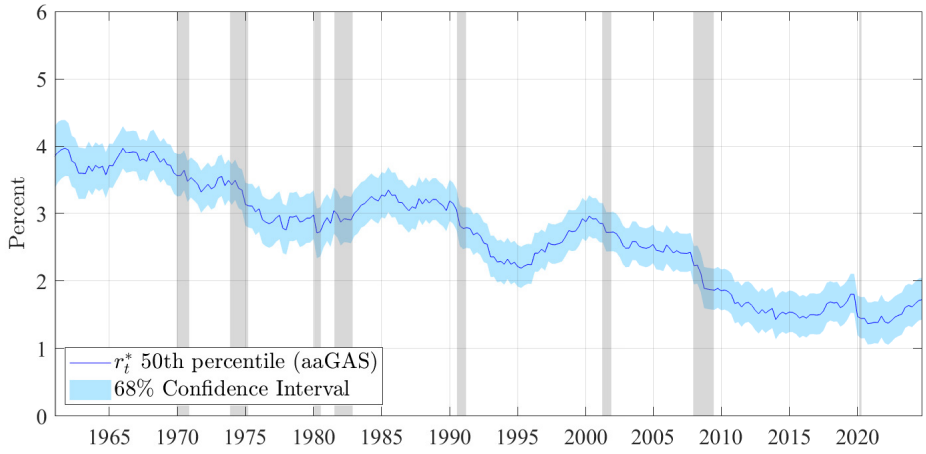

Figure 10: Simulation results for the natural rate of interest using the augmented-accelerating GAS (aaGAS) model. The coloured bands denote the 68% confidence interval corresponding both for filtering and parameter uncertainty. Shaded vertical areas indicate U.S. recessions as dated by the National Bureau of Economic Research (NBER).

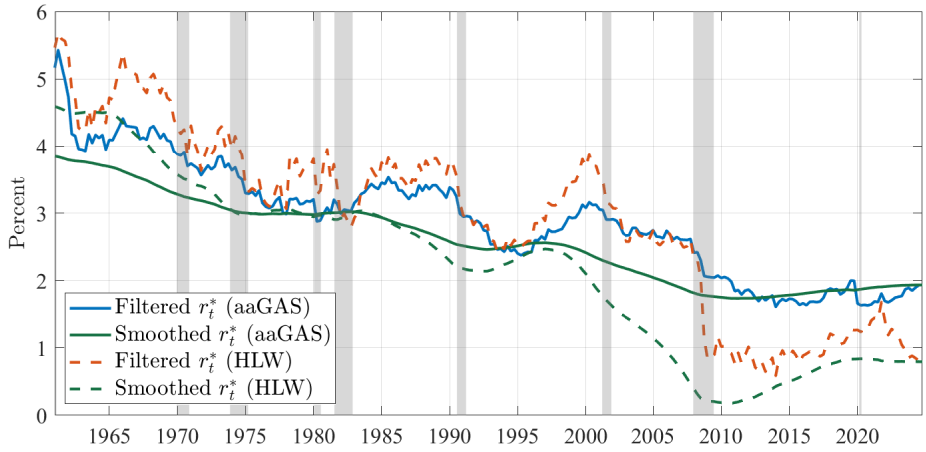

Figure 11: The solid blue line represents the filtered (one-sided) estimates of r-star using the aaGAS model, while the red dashed line shows the corresponding estimates from the HLW approach. The solid green line depicts the smoothed (two-sided) estimates of the natural rate of interest under the aaGAS specification, and the green dashed line shows the smoothed estimates based on the HLW model. Shaded areas indicate U.S. recessions as dated by the National Bureau of Economic Research (NBER).

limited variation in our output. Notably, the two estimates depart significantly after the GFC, with a widening divergence over the rest of the interval. In contrast, as Figure 13 shows, the other determinant of the r-star, the trend growth rate, is characterised by substantially narrower confidence bands and, except for the post-GFC interval, a closer match with the HLW estimate. Overall, these observations, in line with the associated standard errors reported in Table 2, make it evident that most of the uncertainty surrounding the r-star and its higher trajectory over the past two decades relative to the HLW results stems from the estimation of the z-factor. At the same time, as previously discussed, the notably lower standard errors confirm that our models provide a more precise estimation of the z_t compared to HLW, which largely accounts for the reduced uncertainty of our natural rate of interest estimates.

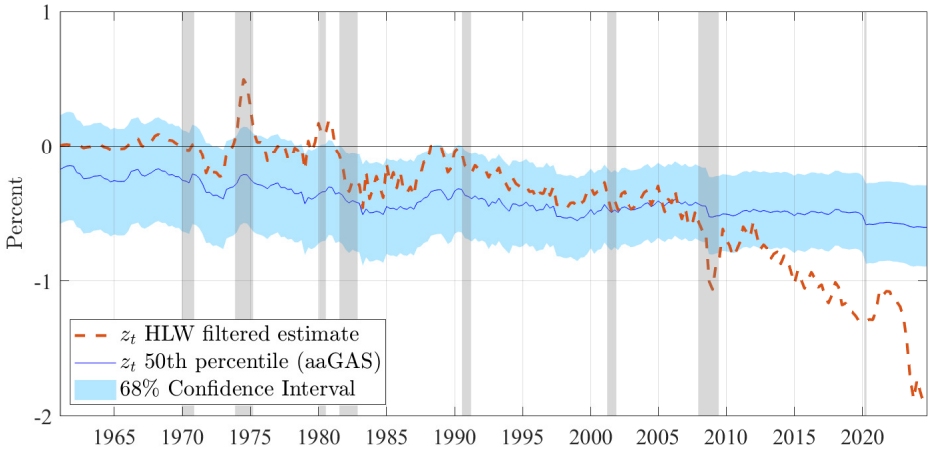

Figure 12: Estimation of the "other factors" component (z_t) by the model with augmented-accelerating GAS (aaGAS) update and with HLW 2023 configuration. The coloured bands denote the 68% confidence interval corresponding both for filtering and parameter uncertainty. Vertical shadows indicate recessions as identified by the National Bureau of Economic Research (NBER).

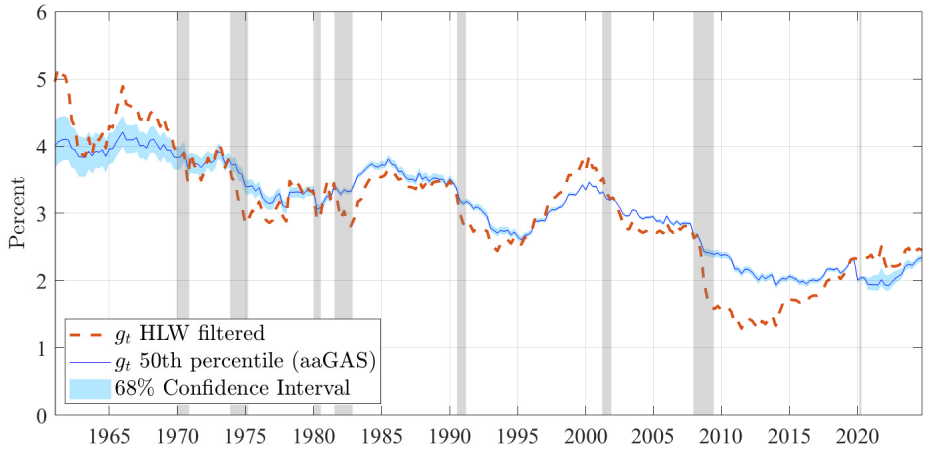

Figure 13: Estimation of the trend growth rate by the model with augmented-accelerating GAS (aaGAS) update and by HLW (2017). The coloured bands denote the 68% confidence interval corresponding both for filtering and parameter uncertainty. Vertical shadows indicate recessions as identified by the National Bureau of Economic Research (NBER).

As discussed before, the key component in the KF algorithm is the Kalman gain matrix, which assigns weights to the prediction errors, determining the latent state. Therefore, it is instructive to examine the evolution of its elements to understand how the score-driven framework influences the estimation via this instrument. We collect the main elements of the Kalman gain matrix in Figure 14, which shows how the weight of the information content in the IS curve (left-hand side column) and the Phillips curve equation (right-hand side column) are allocated through the Kalman filter recursion. While the weights associated with the potential output (upper two panels), and thus determining the output gap, oscillate around the weight obtained from the HLW model, the rest of the panels show a different picture. In particular, the bottom panels in Figure 14 show that the Kalman gains related to the z-factor differ considerably between the two models. Specifically, apart from the periods affected by the COVID-related adjustments, the Kalman gains obtained from the HLW model are consistently higher than those from the

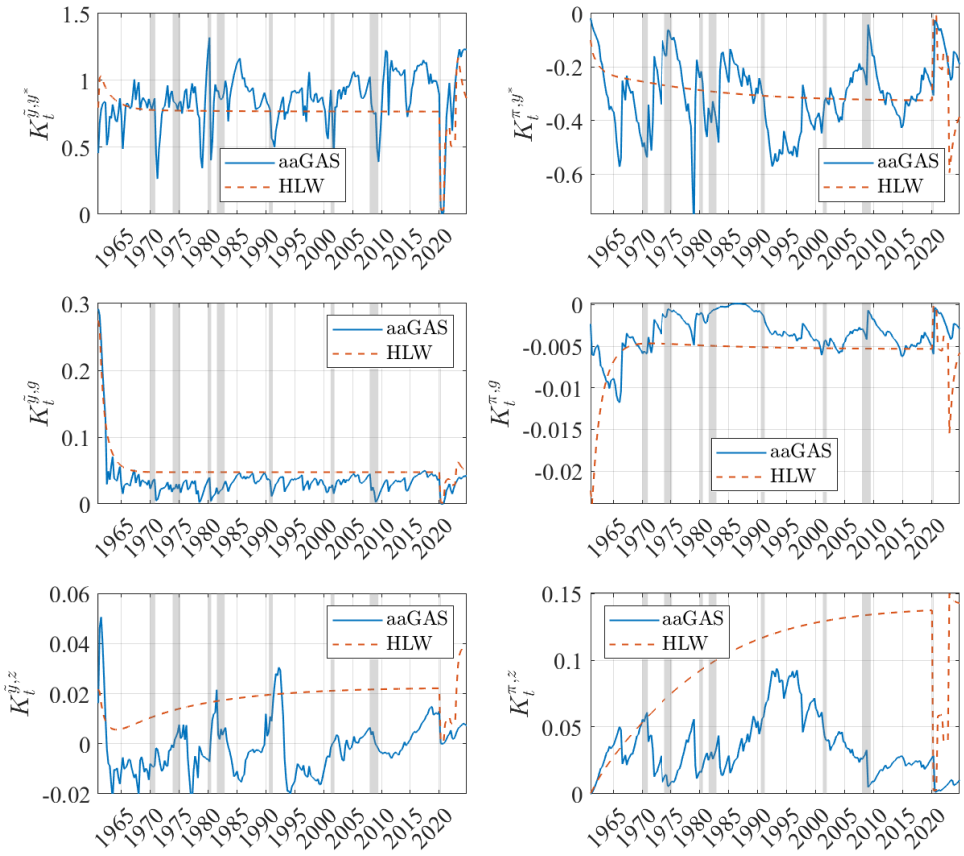

Figure 14: Kalman gains (K_t) associated with different structural equations and state variables. The panels display, from left to right and top to bottom: (1) Kalman gain associated with the potential output and IS equation, (2) Kalman gain associated with the potential output and Phillips curve, (3) Kalman gain associated with the trend growth rate and IS equation, (4) Kalman gain associated with the trend growth rate and inflation dynamics, (5) Kalman gain for the z-factor and IS relation, and (6) Kalman gain for the z-factor and Phillips curve equation.

aaGAS specification. Altogether, the high flexibility provided by the score-driven setup, as opposed to the relatively rigid and larger weights obtained from the static parameter model for the two components of the r-star, g_t and z_t, led to our higher and generally more stable natural rate of interest estimates over the past two decades, materializing primarily through the estimation of the z-factors.

4 Conclusions

Determining the natural rate of interest has been an inspiring subject of academic discourse since the concept was first introduced over a century ago. The present study contributes to this line of research by making the parameters of the Laubach-Williams semi-structural model time-varying, with their dynamics being governed by the conditional likelihood score. In addition, motivated by the econometric challenges initiated by the pandemic, we introduced an augmented accelerating version of the GAS (aaGAS) updating mechanism.

The output gap estimated by the aaGAS suggests that the modified model effectively handles large volatility shifts due to extreme events. Furthermore, the

higher estimate of potential output relative to HLW suggests that the proposed models are more efficient at disentangling transitory and highly persistent shocks, providing some support for Milton Friedman's "plucking model". Regarding the time-varying structural relationships, the IS slope was highly unstable until the beginning of the Great Moderation, gradually flattening during this period and stabilising at a low level after the Great Recession. As for the Phillips curve, while we find little evidence of time variation in its slope parameter, the pronounced downside uncertainty in the simulated parameter limits any decisive conclusions regarding the stability of the slope over the past decades. Most importantly, the r-star estimates exhibit substantially higher precision and reduced variability, along with a flatter downward trend over the analysed interval compared to the benchmark HLW model. In addition, we find that the primary source of the recent divergence in the trajectories and the uncertainty surrounding the natural rate of interest lies in the estimation of the "other factors", z. These state estimates not only deviate substantially from those of HLW but also account for most of the improvement in r-star estimation precision, explaining the higher natural rate of interest—ranging between 1.5% and 2%—observed over the past two decades. Furthermore, the current upward trend in both the filtered and smoothed estimates, in contrast to HLW model output, indicates that the natural rate of interest has already passed its historically low level.

Given the high uncertainty and the ambiguous definition of the z-factor, future research could focus on improving its refined identification and developing more precise specifications. Moreover, considering the low-frequency nature of current estimations and the delayed availability of relevant data, a model that utilizes higher-frequency data and proxy variables could offer a more timely and accurate assessment.

In summary, the lower variability of the r-star estimate, along with the reduced standard errors of the underlying state estimates, implies that the proposed models are more adaptable to sudden changes in the economic environment and, thus, more effective at identifying transitory shocks than the standard LW methodology. Based on a purely statistical, data-driven approach, the GAS (score-driven) models, therefore, provide a valid empirical alternative for estimating the natural rate of interest in real-time, demonstrating a clear advantage in estimation precision. In addition, the aaGAS specification further improves the precision of the r-star estimate, alleviating a long-standing limitation of models based on the LW methodology. Moreover, in light of the occurrence of extreme events in both macroeconomic and financial contexts, the aaGAS offers a viable extension of the standard GAS framework to more adequately model volatility persistence.

References

Ball, L. and S. Mazumder (2011). Inflation Dynamics and the Great Recession. *Brookings Papers on Economic Activity 42*(1 (Spring), 337–405.

Blasques, F., P. Gorgi, and S. Koopman (2019). Accelerating score-driven time series models. *Journal of Econometrics 212*(2), 359–376.

Blasques, F., S. J. Koopman, K. Łasak, and A. Lucas (2016). In-sample confidence bands and out-of-sample forecast bands for time-varying parameters in observation-driven models. *International Journal of Forecasting 32*(3), 875–887.

Bloom, N., P. Bunn, P. Mizen, P. Smietanka, and G. Thwaites (2025). The impact of covid-19 on productivity. *The Review of Economics and Statistics 107*(1), 28–41.

Buncic, D. (2024). Econometric issues in the estimation of the natural rate of interest. *Economic Modelling 132*, 106641.

Creal, D., S. J. Koopman, and A. Lucas (1999). Messy time series. *Advances in Econometrics 13*, 103–143.

Creal, D., S. J. Koopman, and A. Lucas (2013). Generalized autoregressive score models with applications. *Journal of Applied Econometrics 28*(5), 777–795.

Delle Monache, D., I. Petrella, and F. Venditti (2021). Price dividend ratio and long-run stock returns: A score-driven state space model. *Journal of Business & Economic Statistics 39*(4), 1054–1065.

Dupraz, S., E. Nakamura, and J. Steinsson (2019). A Plucking Model of Business Cycles. NBER Working Papers 26351, National Bureau of Economic Research, Inc.

Fernald, J. and H. Li (2022). The impact of covid on productivity and potential output. *Federal Reserve Bank of San Francisco, Working Paper Series 2022*, 01–52.

Friedman, M. (1993). The "plucking model" of business fluctuations revisited. *Economic Inquiry 31*(2), 171–177.

Garnier, J. and B.-R. Wilhelmsen (2009). The natural rate of interest and the financial cycle. *Journal of Economic Behavior Organization 36*.

Gordon, R. (1998). Foundations of the goldilocks economy: Supply shocks and the time-varying nairu. *Brookings Papers on Economic Activity 29*(2), 297–346.

Hamilton, J. D. (1986). A standard error for the estimated state vector of a state-space model. *Journal of Econometrics 33*(3), 387–397.

Harvey, A. C. (1990). *Forecasting, Structural Time Series Models and the Kalman Filter*. Cambridge University Press.

Harvey, A. C. (2013). *Dynamic Models for Volatility and Heavy Tails: With Applications to Financial and Economic Time Series*. Econometric Society Monographs. Cambridge University Press.

Harvey, A. C. and S. J. Koopman (1992). Diagnostic checking of unobserved-components time series models. *Journal of Business Economic Statistics 10*(4), 377–389.

Hazell, J., J. Herreño, E. Nakamura, and J. Steinsson (2022). The slope of the phillips curve: Evidence from u.s. states. *The Quarterly Journal of Economics 137*(3), 1299–1344.

Holston, K., T. Laubach, and J. C. Williams (2017). Measuring the natural rate of interest: International trends and determinants. *Journal of International Economics 108*, S59–S75. 39th Annual NBER International Seminar on Macroeconomics.

Holston, K., T. Laubach, and J. C. Williams (2023). Measuring the natural rate of interest after covid-19. (June 2023).

Inoue, A., B. Rossi, and Y. Wang (2022). Has the phillips curve flattened and why? Number 2022.

Kalman, R. E. (1960). A new approach to linear filtering and prediction problems. *Transactions of the ASME–Journal of Basic Engineering 82*(Series D), 35–45.

Krustev, G. (2019). The natural rate of interest and the financial cycle. *Journal of Economic Behavior Organization 162*, 193–210.

Laubach, T. (2001). Measuring the nairu: Evidence from seven economies. *The Review of Economics and Statistics 83*(2), 218–231.

Laubach, T. and J. C. Williams (2003). Measuring the natural rate of interest. *The Review of Economics and Statistics 85*(4), 1063–1070.

Staiger, D., J. H. Stock, and M. W. Watson (1996). How precise are estimates of the natural rate of unemployment? Working Paper 5477, National Bureau of Economic Research.

Stock, J. H. (1994). Unit roots, structural breaks and trends. Volume 4 of *Handbook of Econometrics*, pp. 2739–2841. Elsevier.

Stock, J. H. and M. W. Watson (1998). Median unbiased estimation of coefficient variance in a time-varying parameter model. *Journal of the American Statistical Association 93*(441), 349–358.

Suah, J. L. (2024). The "plucking" model of the unemployment rate floor: Corss-country estimates and empirics. BIS Working Papers 1159, Bank for International Settlements.

Taylor, J. B. (1993). Discretion versus policy rules in practice. *Carnegie-Rochester Conference Series on Public Policy 39*, 195–214.

Wicksell, K. (1936). *Interest and Prices: A Study of the Causes Regulating the Value of Money*. Macmillan. Originally published in German as *Geldzins und Güterpreise* in 1898.

Appendix

A. Time-Varying AR Update in the aaGAS

Assuming $\partial \lambda_{t-1} / \partial f_t = 0$,

$$
\begin{aligned}
\frac{\partial \log(p)}{\partial g_t} &= \frac{\partial \log(p)}{\partial \lambda_t}\frac{\partial \lambda_t}{\partial g_t} \\
&= u_{\lambda,t}\frac{\partial \lambda_t}{\partial g_t} = u_{\lambda,t}\left(\mathrm{b}_{\lambda,t-1}\frac{\partial \lambda_{t-1}}{\partial g_t}\mathrm{a}_{\lambda,t}\frac{\partial s_{\lambda,t-1}}{\partial g_t}\right) \\
&= u_{\lambda,t}\left(\frac{\partial \mathrm{b}_{\lambda,t-1}}{\partial g_t}\lambda_{t-1}\right) \\
&\propto u_{\lambda,t}\lambda_{t-1},
\end{aligned}
$$

where

$$
u_{g,t} = \frac{\partial \log p(y_t \mid \lambda_t; \theta)}{\partial g_t} \propto u_{\lambda,t}\lambda_{t-1}.
$$

B. Additional derivations and matrix representation of the estimated models

The time-varying parameters collected in λ_t are governed by the score-driven framework outlined in Section 2.3, where the components in Eq. 13 are specified as:

$$
\begin{aligned}
\omega_\lambda &= \left[\omega_{\tilde{y}}, \quad \omega_\pi, \quad \omega_{y^*}, \quad 0, \quad 0\right]', \\
\mathbf{A}_\lambda &= \mathrm{diag}\left(\left[\mathrm{a}_{\sigma_{\tilde{y}}}, \quad \mathrm{a}_{\sigma_\pi}, \quad \mathrm{a}_{\sigma_{y^*}}, \quad \mathrm{a}_{y^*}, \quad \mathrm{a}_\pi\right]\right), \\
\mathbf{B}_\lambda &= \mathrm{diag}\left(\left[\mathrm{b}_{\sigma_{\tilde{y}}}, \quad \mathrm{b}_{\sigma_\pi}, \quad \mathrm{b}_{\sigma_{y^*}}, \quad \mathrm{b}_{y^*}, \quad \mathrm{b}_\pi\right]\right)
\end{aligned}
$$

where, in the aaGAS model, the parameter $\mathrm{a}_{\sigma_{\tilde{y}}}$ and $\mathrm{b}_{\sigma_{\tilde{y}}}$ becomes time-varying governed by Eq. 16.

Time variation in the input matrix Γ evolves through the equation

$$
vec(\Gamma_t) = S_{0,\Gamma} + S_{1,\Gamma}\psi(S_{2,\Gamma}\lambda_t),
$$

where the components take the following forms:

$$
vec(\Gamma_t) = \begin{bmatrix} a_1 \\ b_{\pi,t} \\ a_2 \\ 0 \\ a_{\tilde{y},t}/2 \\ 0 \\ a_{\tilde{y},t}/2 \\ 0 \\ 0 \\ b_1 \\ 0 \\ (1-b_1) \end{bmatrix}, \qquad S_{0,\Gamma} = \begin{bmatrix} a_1 \\ 0 \\ a_2 \\ 0 \\ 0 \\ 0 \\ 0 \\ 0 \\ 0 \\ b_1 \\ 0 \\ (1-b_1) \end{bmatrix}, \qquad S_{1,\Gamma} = \begin{bmatrix} 0 & 0 & 0 \\ 0 & 1 & 0 \\ 0 & 0 & 0 \\ 0 & 0 & 0 \\ 1 & 0 & 0 \\ 0 & 0 & 0 \\ 0 & 0 & 1 \\ 0 & 0 & 0 \\ 0 & 0 & 0 \\ 0 & 0 & 0 \\ 0 & 0 & 0 \\ 0 & 0 & 0 \end{bmatrix},
$$

$$\psi_\Gamma = \begin{bmatrix} a_{\tilde{y},t}/2 \\ b_{\pi,t} \\ a_{\tilde{y},t}/2 \end{bmatrix}, \qquad S_{2,\Gamma} = \begin{bmatrix} 0 & 0 & 0 & 1 & 0 \\ 0 & 0 & 0 & 0 & 1 \end{bmatrix}.$$

The Jacobian matrix is:

$$\dot{\Gamma}_t = S_{1,\Gamma} \dot{\Psi}_{\Gamma,t} S_{2,\Gamma},$$

where

$$\dot{\Psi}_{\Gamma,t} = \frac{\partial \psi(S_{2,\Gamma}\lambda_t)}{\partial \lambda_t'} = \frac{\partial \psi_{\Gamma,t}(S_{2,\Gamma}\lambda_t)}{\partial (S_{2,\Gamma}\lambda_t)'} \frac{\partial (S_{2,\Gamma}\lambda_t)}{\partial \lambda_t'} = \begin{bmatrix} a_{\tilde{y},t}/2 & 0 \\ 0 & b_{\pi,t} \\ a_{\tilde{y},t}/2 & 0 \end{bmatrix}.$$

Time variation in the system matrix Z evolves through the equation

$$vec(Z_t) = S_{0,Z} + S_{1,Z}\psi(S_{2,Z}\lambda_t),$$

where

$$vec(Z_t) = \begin{bmatrix} 1 \\ 0 \\ -a_1 \\ -b_{\pi,t} \\ -a_2 \\ 0 \\ 0 \\ 0 \\ -a_{\tilde{y},t} \cdot 2 \\ 0 \\ -a_{\tilde{y},t} \cdot 2 \\ 0 \\ 0 \\ 0 \\ -a_{\tilde{y},t}/2 \\ 0 \\ -a_{\tilde{y},t}/2 \\ 0 \end{bmatrix}, \qquad S_{Z,0} = \begin{bmatrix} 1 \\ 0 \\ -a_1 \\ 0 \\ -a_2 \\ 0 \\ 0 \\ 0 \\ 0 \\ 0 \\ 0 \\ 0 \\ 0 \\ 0 \\ 0 \\ 0 \\ 0 \\ 0 \end{bmatrix}, \qquad S_{Z,1} = \begin{bmatrix} 0 & 0 & 0 & 0 & 0 \\ 0 & 0 & 0 & 0 & 0 \\ 0 & 0 & 0 & 0 & 0 \\ 0 & 1 & 0 & 0 & 0 \\ 0 & 0 & 0 & 0 & 0 \\ 0 & 0 & 0 & 0 & 0 \\ 0 & 0 & 0 & 0 & 0 \\ 0 & 0 & 0 & 0 & 0 \\ 1 & 0 & 0 & 0 & 0 \\ 0 & 0 & 0 & 0 & 0 \\ 0 & 0 & 1 & 0 & 0 \\ 0 & 0 & 0 & 0 & 0 \\ 0 & 0 & 0 & 0 & 0 \\ 0 & 0 & 0 & 0 & 0 \\ 0 & 0 & 0 & 1 & 0 \\ 0 & 0 & 0 & 0 & 0 \\ 0 & 0 & 0 & 0 & 1 \\ 0 & 0 & 0 & 0 & 0 \end{bmatrix},$$

$$\psi_Z = \begin{bmatrix} -a_{\tilde{y},t} \cdot 2 \\ -b_{\pi,t} \\ -a_{\tilde{y},t} \cdot 2 \\ -a_{\tilde{y},t}/2 \\ -a_{\tilde{y},t}/2 \end{bmatrix}, \qquad S_{Z,2} = \begin{bmatrix} 0 & 0 & 0 & 1 & 0 \\ 0 & 0 & 0 & 0 & 1 \end{bmatrix}.$$

The Jacobian matrix is:

$$\dot{Z}_t = S_{1,Z}\dot{\Psi}_{Z,t}S_{2,Z},$$

$$\dot{\Psi}_{Z,t} = \frac{\partial\psi(S_{2,Z}\lambda_t)}{\partial\lambda_t'} = \frac{\partial\psi_{Z,t}(S_{2,Z}\lambda_t)}{\partial(S_{2,Z}\lambda_t)'}\frac{\partial(S_{2,Z}\lambda_t)}{\partial\lambda_t'} = \begin{bmatrix} -a_{\tilde{y},t}\cdot 2 & 0 \\ 0 & -b_{\pi,t} \\ -a_{\tilde{y},t}\cdot 2 & 0 \\ -a_{\tilde{y},t}/2 & 0 \\ -a_{\tilde{y},t}/2 & 0 \end{bmatrix}.$$

Time variation in the system matrix H is defined as

$$vec(H_t) = S_{0,H} + S_{1,H}\psi_H(S_{2,H}\lambda_t),$$

where

$$vec(H_t) = \begin{bmatrix} \sigma_{\tilde{y},t} \\ 0 \\ 0 \\ \sigma_{\pi,t} \end{bmatrix}, \qquad S_{0,H} = \begin{bmatrix} 0 \\ 0 \\ 0 \\ 0 \end{bmatrix}, \qquad S_{1,H} = \begin{bmatrix} 1 & 0 \\ 0 & 0 \\ 0 & 0 \\ 0 & 1 \end{bmatrix},$$

$$\psi_H = \begin{bmatrix} \sigma_{\tilde{y},t} \\ \sigma_{\pi,t} \end{bmatrix}, \qquad S_{2,H} = \begin{bmatrix} 1 & 0 & 0 & 0 & 0 \\ 0 & 1 & 0 & 0 & 0 \end{bmatrix}.$$

The Jacobian matrix is:

$$\dot{H}_t = S_{1,H}\dot{\Psi}_{H,t}S_{2,H},$$

$$\dot{\Psi}_{H,t} = \frac{\partial\psi(S_{2,H}\lambda_t)}{\partial\lambda_t'} = \frac{\partial\psi_{H,t}(S_{2,H}\lambda_t)}{\partial(S_{2,H}\lambda_t)'}\frac{\partial(S_{2,H}\lambda_t)}{\partial\lambda_t'} = \begin{bmatrix} \sigma_{\tilde{y},t} & 0 \\ 0 & \sigma_{\pi,t} \end{bmatrix}.$$

Time variation in the system matrix Q follows as

$$vec(Q_t) = S_{0,Q} + S_{1,Q}\psi_Q(S_{2,Q}\lambda_t),$$

where

$$vec(Q_t) = \begin{bmatrix} \sigma_{y^*,t} \\ 0_{(29\times 1)} \\ \sigma_g \\ 0_{(29\times 1)} \\ \sigma_z \\ 0_{(20\times 1)} \end{bmatrix}, \qquad S_{0,Q} = \begin{bmatrix} 0_{(30\times 1)} \\ \sigma_g \\ 0_{(29\times 1)} \\ \sigma_z \\ 0_{(20\times 1)} \end{bmatrix}, \qquad S_{1,Q} = \begin{bmatrix} 1 \\ 0_{(80\times 1)} \end{bmatrix},$$

$$\psi_Q = \left[\sigma_{y^*,t}\right], \qquad S_{2,Q} = \begin{bmatrix} 0 & 0 & 1 & 0 & 0 \end{bmatrix}.$$

The Jacobian matrix is:

$$\dot{Q}_t = S_{1,Q}\dot{\Psi}_{Q,t}S_{2,Q},$$

$$\dot{\Psi}_{Q,t} = \frac{\partial \psi(S_{2,Q}\lambda_t)}{\partial \lambda_t'} = \frac{\partial \psi_{Q,t}(S_{2,Q}\lambda_t)}{\partial (S_{2,Q}\lambda_t)'}\frac{\partial (S_{2,Q}\lambda_t)}{\partial \lambda_t'} = \sigma_{y^*,t}.$$

The Jacobian associated with the prediction errors takes the form:

$$\dot{V}_t = \frac{\partial v_t}{\partial \lambda_t'} = \left[\frac{\partial v_t}{\partial \mathrm{vec}(Z_t)'}\frac{\partial \mathrm{vec}(Z_t)}{\partial \lambda_t'} + \frac{\partial v_t}{\partial \alpha_t'}\frac{\partial \alpha_t}{\partial \lambda_t'} + \frac{\partial v_t}{\partial \mathrm{vec}(\Gamma_t)'}\frac{\partial \mathrm{vec}(\Gamma_t)}{\partial \lambda_t'}\right]$$

$$= -\left[(\alpha_t' \otimes I_n)\frac{\partial\, \mathrm{vec}(Z_t)}{\partial \lambda_t'} + Z_t \otimes \frac{\partial \alpha_t}{\partial \lambda_t'} + (u_t' \otimes I_n)\frac{\partial\, \mathrm{vec}(\Gamma_t)}{\partial \lambda_t'}\right]$$

$$= -\left[(\alpha_t' \otimes I_n)\dot{Z}_t + (u_t' \otimes I_n)\dot{\Gamma}_t\right], \; n = 2.$$